UCLA
UCLA Electronic Theses and Dissertations

Title
Determination of Functional Activity of Sodium Glucose Transporters in Cancer

Permalink
https://escholarship.org/uc/item/1rj3h2xh

Author
Silverman, Matthew John

Publication Date
2014

Peer reviewed|Thesis/dissertation

UNIVERSITY OF CALIFORNIA

Los Angeles

Determination of Functional Activity of Sodium Glucose Transporters in Cancer

A dissertation submitted in partial satisfaction of the requirements for the degree of Doctor of Philosophy in Chemical Engineering

By

Matthew John Silverman

2014

ABSTRACT OF THE DISSERTATION

Determination of Functional Activity of Sodium Glucose Transporters in Cancer

By

Matthew John Silverman

Doctor of Philosophy in Chemical Engineering

University of California, Los Angeles, 2014

Professor Jorge Barrio and Professor James Liao, Co-chairs

As cancer incidence continues to rise in the United States, there remains an increasing demand
for new tools for oncologists to use for both diagnosing and directing treatments for cancer.
Among these tools, Positron Emission Tomography (PET) has been rising in prominence in recent
decades as a useful tool for monitoring the metabolic activity of organs and tissues *in vivo*.
Unlike Computed Tomography (CT), Magnetic Resonance Imaging (MRI) or Ultrasound (US), PET
imaging allows medical professionals and researchers to use molecular imaging probes to
measure metabolic activity of tissues, opening up a different dimension of medical evaluation.
In PET imaging for cancer, 2-deoxy-2-[F-18]fluoro-D-glucose (2-FDG) has been the historically
dominant molecular probe used, since 2-FDG uptake occurs via facilitative glucose transporters
(GLUTs), and its tissue accumulation reflects hexokinase (HK) activity in proportion to the
glucose metabolic rate. In many cancers, glucose utilization through these transporters
increases dramatically relative to non-cancerous tissue, making 2-FDG a valuable molecular
imaging probe in detecting and monitoring the progression of cancer. However, there are some
cancers that don't show consistently increased 2-FDG uptake, rendering 2-FDG PET less effective
in these situations for medical diagnosis. Recent work has suggested the possibility that another
class of glucose transporters, sodium glucose transporters (SGLTs), is expressed and active in a

variety of cancers. SGLT activity, which cannot be measured by 2-FDG PET, could offer an explanation as to why 2-FDG accumulation seems less significant in some cancers. While there have been several publications examining mRNA and protein SGLT expression in cancer, there has yet to be any data confirming functional SGLT activity *in vivo*. In this work, we present initial data on the functional activity of SGLTs in cancerous cells from both prostate and pancreatic cancer both *in vitro* and *in vivo*. Using methyl-4-deoxy-4-[F-18]fluoro-D-glucopyranoside (Me-4FDG), a PET molecular imaging probe specific for SGLTs, we identify SGLT activity in cancer cell lines, animal tumor xenografts, and human tumors. These results usher in the novel possibility of utilizing SGLT PET imaging molecular imaging probes for diagnosing and characterizing cancerous tumors.

The dissertation of Matthew John Silverman is approved.

Harold G. Monbouquette

James C. Liao, Committee Co-chair

Jorge R. Barrio, Committee Co-chair

University of California, Los Angeles

2014

Table of Contents

List of Figures

Curriculum Vita

Education:

M.S., Chemical and Biomolecular Engineering, March 2010, UCLA

> Thesis: Use of Branched Chain Alpha Keto Acid Dehydrogenase Complex for Fusel Alcohol Fermentation

B.S., Chemical Engineering (Biomedical Engr. emphasis), June 2006, UCLA

Fellowships:

> NSF GK-12 Graduate STEM Fellow

Work experience:

Chemistry Teacher: Village Christian High School

Teaching Assistant: UCLA School of Engineering
-Transport Phenomena
-Process Control
-Plant Design
-Technology Management

Engineering Intern –Semiconductor manufacturing: AMD Spansion, Sunnyvale, CA

Boy Scouts of America, Eagle Scout

1 Purpose and Organization of the Investigation

1.1 Cancer Mortality

Despite decades of research and the development of new drugs and treatments, cancer remains a leading cause of mortality in the United States, second only to heart disease. In the 2013 annual Cancer Facts and Figures Report, the American Cancer Society estimates there will be five hundred eighty thousand deaths from cancers in 2013 in the United States. Estimated mortalities for some of the most lethal cancers are shown in Figure 1. While new treatments are constantly in development, improved diagnostic tools remain in high demand for many cancers.

Most cancers are highly treatable if caught early, but difficulty in diagnosis due to lack of unique symptoms leaves these cancers undetected for months. Even once they are detected, the inability to monitor the progression of certain cancers makes it difficult to quickly evaluate the effectiveness of treatments. For many cancers, simply identifying whether or not the disease has metastasized to local regions remains a challenge, despite being crucial for directing effective treatment.

Lung & Bronchus
159k

Brain
14k

Digestive System
145k

Breast
40k

Urinary System
40k

Ovarian
14k

Prostate
30k

Total
580k
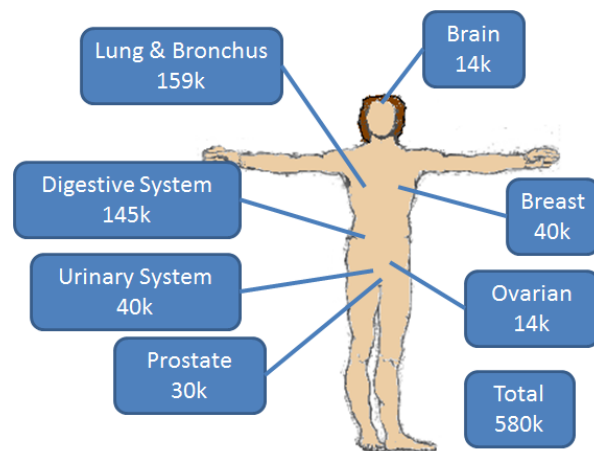
Figure 1: Estimated 2013 mortalities for selected cancers

Among the most difficult cancers for both imaging and treatment are pancreatic and prostate cancers. Treatment for each of these cancers benefits tremendously from early detection, yet reliable early detection methods are lacking. As indicated in Figure 2, pancreatic cancer has high mortality, but only when not identified in early stages. Prostate cancer has high survivability,

Pancreatic: 6%

Liver: 15%

Lung: 16%

Esophagus: 17%

Brain: 35%

Ovarian: 44%

Leukemia: 58%

Colon/Rectal: 64%

Non-Hodgkin Lymphoma: 71%

Bladder: 78%

Breast: 89%

Prostate: 99%
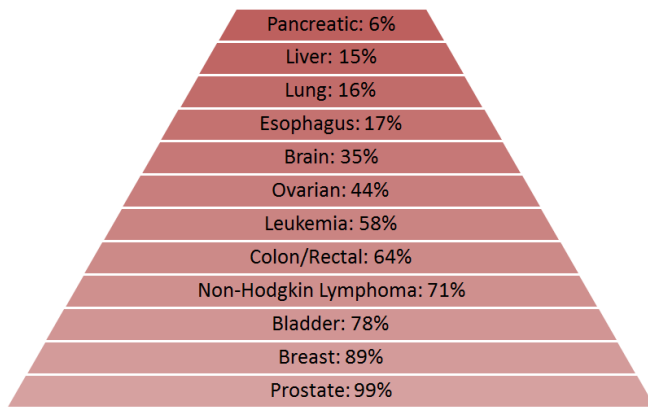
Figure 2: Five year survival rates from 2002 to 2008 for top twelve lethal cancers, averaged over all stages, ranked from lowest survival to highest. While these cancer represent the highest mortalities due to cancer in the United States, they vary greatly in patient response to current treatments available. Five year survival rates are much higher for cancers diagnosed at lower stages, making early, accurate detection an essential tool for oncologists.

even in more advanced stages, but difficulties identifying relapse make it challenging in establishing proper treatments. As such, new imaging options are in high demand for these cancers in particular. Improved imaging options can allow more effective diagnosis and staging, directing both surgery and treatment options.

1.1.1 Background on Pancreatic Cancer

Over the last decade, pancreatic cancer has been estimated to be diagnosed in over thirty thousand individuals in the United States each year[1–3], with a 5 year survival rate around 6% and a projected 38,460 deaths in 2013 according to the 2013 Cancer Facts & Figures publication by the American Cancer Society. Currently, complete resection of the tumor before metastasis is the only option for long term survival. Unfortunately, due to poor methods of detection, most cases aren't diagnosed until metastasis has already occurred, eliminating the potential for resection[4].

Pancreatic cancer is staged at 4 levels, using either the Japan Pancreas Society (JPS) or the Union Internationale Contre le Cancer (UICC) conventions. Staging is based on tumor size, lymph node metastasis, and distant metastasis. Stage 1 corresponds to a tumor less than 2cm in size, while stages 2 and 3 correspond to larger tumors that have spread to nearby lymph nodes. Stage 4 corresponds to cancer with any level of metastasis beyond the pancreas.[5]

Pancreatic cancer is often not diagnosed until it has reached a late stage. In one analysis of symptoms associated with pancreatic cancer, around 5% of patients had no symptoms when diagnosed, while close to 50% had no more than abdominal pain[6]. Other symptoms included indigestion, jaundice, and weight loss. Not only are symptoms often lacking; they tend to overlap with symptoms of many other pancreatic diseases, such as pancreatitis[7,8]. As a result, there are many ongoing trials searching for markers and imaging techniques that can identify pancreatic cancer at early development.

Biomarkers (proteins or other small molecules circulating in the blood) are one of the most useful tools for diagnosing cancer in that they can be easily measured during a regular blood or urine test and used as an indicator of whether or not to conduct further tests looking for the presence of cancer. Since cancer cells tend to exhibit altered cellular activity, peptides, glycoconjugates, and other biological molecules are often excreted at altered levels, changing the observed levels of that particular molecule in the blood or urine. A large number of markers have been identified to often have elevated concentrations in individuals with pancreatic cancer, including carbohydrate antigen 19-9, 50, and 242 (CA19-9, CA-50, CA242), carcinoembryonic antigen (CEA), Claudin 18, Annexin A8, PEDF, βIGH3, Thrombospondin-2, Biglycan, SPAN-1, Dupan-2, and elastase-1[9–11]. Large scale proteomic profiling is also increasingly being used to search through large numbers of molecules as potential biomarkers[12]. Unfortunately, these markers aren't universal indicators of the presence of pancreatic cancer, often only being elevated once the disease has progressed to a later stage. Markers can also present a false positive, ultimately requiring imaging and biopsy for final diagnosis. For this reason, they tend to be monitored primarily in either high risk individuals or patients who have already had cancer, used to identify signs of relapse or response to treatment[13].

1.1.2 Background on Prostate Cancer

Statistically, 1 out of every 6 men will be diagnosed with prostate cancer, with 20-30% of those diagnosed presenting with advanced stage[14]. Traditionally, the primary methods of screening are through either a prostate exam or screening for prostate-specific antigen (PSA). When diagnosed in an early stage, the survival rate of prostate cancer is almost 100%, and most metastases will respond initially to androgen withdrawal. Unfortunately, metastatic cases will usually return within 2 years, resistant to hormonal treatment[15,16]. In addition, PSA has proven to be a less than ideal marker; despite being approved by the FDA for prostate cancer screening since 1994, there is a significant lack of evidence that PSA screening results in any decline in mortality[17]. A recent randomized study of 76,693 men found that annual PSA screening for 6 years and digital rectal exam for 4 years together offered no noticeable survival benefit for the screening group over the control group[18]. Dozens of biomarkers based on different aspects of cancer biology have been explored for potential use in diagnostic and prognostic evaluation, yet none currently demonstrate the level of sensitivity and specificity necessary for directing choice and course of treatment[17]. With this in mind, trials are also being done utilizing several biomarkers together to increase accuracy. A recent pilot study of 45 men seeking to optimize usage of biomarkers showed low sensitivity for PSA alone, while testing urine samples from the same men for expression of prostate cancer gene 3 (PCA3) and the gene fusion TMPRSS2:ERG using quantitative RT-PCR showed improved sensitivity (93% for PCA3 and 67% for TMPRSS2:ERG), but poorer specificity. The results identified an optimized combination of using all three markers to maximize both sensitivity and specificity for directing biopsy[19]. Despite this combination, the optimized algorithm still only had a sensitivity of 80%, failing to direct biopsy in 3 of the 15 patients presenting with prostate cancer. With a high inconvenience associated with

invasive surgeries resulting from false positives from biomarkers, improved methods for detecting

and staging prostate cancer are in high demand.

1.2 Cancer metabolism

One of the most distinguishing marks of cancer over the past century has been the observation of increased glucose utilization. In particular, cancers are known to have increased glycolytic activity and lactate production, even in the presence of sufficient oxygen for aerobic respiration. In some cases, this increase in aerobic glycolysis has been associated with more aggressive cancers and poor clinical outcomes, although there are exceptions to that trend[20].
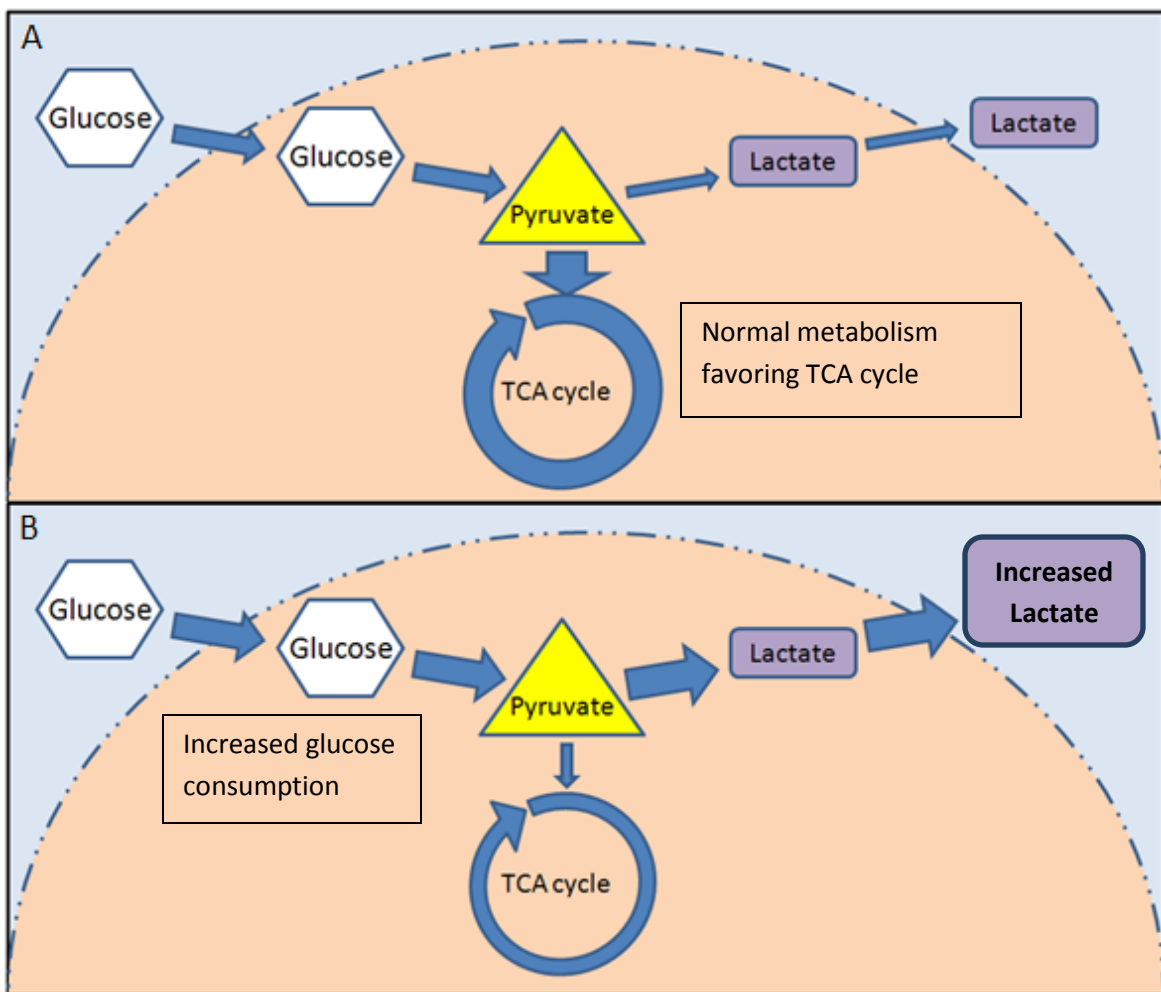
Figure 3: Cancer metabolism switches from a normal cellular metabolism (A) that favors metabolism via the TCA cycle to aerobic glycolysis (B) that favors the production of lactate from glucose. This observation, known as the Warburg Effect, is a distinguishing mark of cancer.

Working off of the assumption that this increased glycolytic metabolism offers some crucial benefit to cancer survival, there have been many attempts to treat cancer by inhibiting glucose uptake or metabolism. Molecules such as 2-deoxy-D-glucose (2DG), Phloretin, and Silybin have been tested for inhibiting glucose uptake via the passive glucose transporters (GLUTs), in the hopes of inducing starvation in cancer cells. GLUT1 and GLUT3 in particular, both high affinity glucose transporters that have been found upregulated in cancer, were attractive targets[21]. Other steps of the glycolytic pathway have also been targeted, with molecules inhibiting hexokinase, phosphofructokinase, pyruvate kinase, lactate dehydrogenase, pyruvate dehydrogenase, and even the lactate transporter MCT1. Several regulatory proteins connected to cellular energy and metabolism have also been targets for treatment, such as hypoxia inducible factors, c-Myc, and AMP-activated protein kinase[21].

Unfortunately, there are several factors currently hindering attempts to develop cancer treatments targeting increased glycolysis in cancer. One disadvantage is the glycolytic pathway is essential in virtually all cells, making it difficult to target a treatment that affects only cancer when inhibiting glucose metabolism. Additionally, many glycolysis intermediates are small, very polar molecules, leaving most glycolytic enzymes with small active sites that are difficult to target with selective inhibitors[22]. Consequently, there is still great difficulty in developing treatments for cancer based on metabolic activity, despite the enormous promise in treatments. Identifying crucial metabolic steps that are unique to cancer and easy to target with inhibitors will be extremely important in the years to come, with the potential to greatly reduce costs and mortality in cancer treatment.

1.3 Role and Limitations of Cancer Imaging

While initial diagnosis of cancer is often dependent on distinctive symptoms, such as pain, lumps, or elevated biomarkers in the blood or urine, establishing the grade and locations of the tumors is essential for guiding treatment. For this, either accurate imaging or exploratory surgery is needed. Although techniques for more accurate and less invasive surgeries are constantly being developed, surgery is still less effective for identifying metastasis to unsuspected regions, and often remains invasive. Thus, reliable imaging remains essential in directing treatment after initial suspicion of cancer, and many imaging technologies have been used for detecting a variety of different cancers.

1.3.1 Imaging in Pancreatic Cancer

A common method of detecting pancreatic cancer is using ultrasound (US). For pancreatic cancer In particular, the procedure of choice is endoscopic ultrasound, which utilizes an endoscope inserted into the digestive tract through the esophagus, generating an ultrasound image of the pancreas to identify any lesions or abnormalities[23]. While US alone is useful for distinguishing solid masses in the pancreas, it isn't particularly useful for distinguishing between benign masses and cancer tumors[24], leaving doctors to continue relying on biopsy for final diagnosis. However, the endoscope can also be used to guide a small needle for a biopsy of the abnormality, a procedure called endoscopic ultrasound guided fine needle aspiration biopsy (EUS-FNA), allowing for an efficient combination of the two

Figure 4: Example of endoscopic ultrasound image of insulinoma tumor in body of pancreas[25]. Ultrasound can be a useful tool in imaging the pancreas, but can't be used for detecting metastasized cancer.

8

techniques. Using endoscopic ultrasound also has the benefit of being able to detect smaller tumors than CT or MRI scans, generally improving accuracy of diagnosis[25].

Multidetector spiral computed tomography (MSCT), utilizing contrast that allows identification of digestive organs, has recently started to prove more accurate in diagnosing and staging pancreatic cancer[26]. Since this procedure is often more readily available than EUS-FNA, it has become a more widely used procedure for diagnosis. A recent analysis involving 81 patients comparing MSCT to EUS-FNA found MSCT to correctly identify pancreatic cancer in 53 out of 71 patients, and correctly rule out pancreatic cancer in 7 of the 10 patients. EUS-FNA correctly identified 63 of the patients that had pancreatic cancer, and ruled out all 10 that didn't[26].

There are a variety of other imaging technologies that are used for diagnosing pancreatic diseases, although not used specifically for cancer. Endoscopic retrograde cholangio-pancreatography (ERCP) has been widely used as the primary tool for imaging of biliary-pancreatic diseases, using a contrast enhanced CT x-ray scan. An early evaluation comparing ERCP to other examination methods In 85 patients with either pancreatic cancer or pancreatitis found ERCP to be able to properly identify pancreatic cancer in 84% of patients, and properly identify pancreatitis in 55%[27]. MRI is also used in the diagnosis of many medical conditions, offering the benefit of imaging without the use of ionizing radiation needed for x-rays, CT, or PET scans, although health concerns can arise from the use of contrast in imaging in rare occasions, limiting the use in some patients[28]. Magnetic resonance cholangiopancreatography (MRCP) is a method of imaging the abdomen using MRI without contrast[29], and in one study of 124 patients, correctly identified 31 out of 37 patients who had pancreatic cancer, while 26 out of 37 were identified by ERCP. MRCP was also useful in distinguishing between pancreatic cancer and chronic pancreatitis,

showing a specificity of 96.6% in diagnosing pancreatic carcinoma and 94% in diagnosing chronic pancreatitis[30]. Tests of these imaging techniques for cancer remain limited, however, and aren't typically used specifically for cancer diagnosis.

Single photon emission computed tomography (SPECT) and positron emission tomography (PET) are both uniquely beneficial in cancer diagnosis and monitoring in that they allow for the detection of not only the presence of cancer, but also specific biological functions such as receptor or transporter activity[31,32]. These techniques rely on altered protein activity in cancer tumors, taking up larger amounts of an injected radioactive molecular imaging probe than surrounding tissues and organs. The photons emitted by the radioactive decay of these molecules can then be detected and used to pinpoint the areas of abnormality. The radiolabeled molecules are typically similar or identical to normal cell substrates, such as glucose or acetate, but with one atom replaced with an isotope that decays radioactively within a span of a few hours.

2-FDG PET is particularly useful in detecting cancer due to the increased glycolytic metabolism typically associated with cancer cells. Since tumors uptake the radiolabeled 2-FDG in much higher quantities than surrounding tissue, PET scans can easily identify tumors in the body. The biggest limitation in this technique is the lack of significant anatomic information in PET scans, making it difficult to locate the tumor with respect to surrounding organs[33].

This limitation is often overcome by the combination of CT and PET scans; overlapping the images to get a picture both of the anatomy of the area and the presence of altered metabolism. In one study of 38 patients with suspicion of pancreatic tumor, combined 2-FDG-PET/CT was able to identify pancreatic cancer in 17 out of the 20 patients with cancer and correctly ruled out cancer in 17 of the 18 patients that did not have cancer. In total, PET/CT demonstrated an

accuracy of 89%, compared with an accuracy of 79% for MRI. PET/CT showed less accuracy in identifying metastasis to nearby lymph nodes, however, underestimating metastasis in 5 out of the 8 patients with metastasis in lymph nodes, results that were similar to the other imaging methods tested[34].

Other molecular imaging probes are currently in use or are being developed for use in pancreatic cancer, with varying degrees of success. The thymidine analog [F-18]-fluorothymidine (FLT) has been increasingly used in cancer imaging, taking advantage of increased DNA replication in proliferating cells. Initial attempts to use FLT for imaging pancreatic cancer met with poor success, with only 2 of the 5 cancer patients studied demonstrating a sufficient signal to be used in diagnosis. FLT also had poor specificity, with several spots detected in the PET image in areas that didn't contain tumors[35]
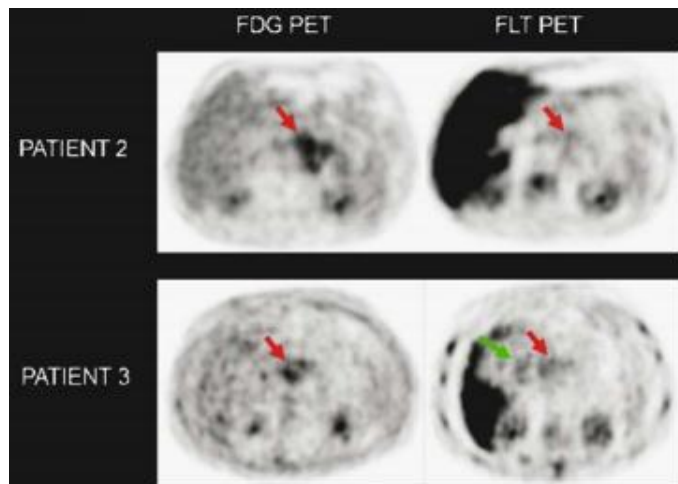
Figure 5: PET scans comparing FDG (left) and FLT (right) in detecting pancreatic cancer. Results of tests comparing FDG and FLT in 5 patients showed poor performance of FLT, with weaker signals in detecting tumors (red arrows) and false signals not related to cancer (green arrow)[35].

All in all, significant progress has been made in developing imaging methods for detecting pancreatic cancer, but there is still no universally reliable screening method that works for all forms of pancreatic cancer. Considering the high mortality of pancreatic cancer, there remains a great desire to develop an imaging technique that can reliably identify early tumors for surgical removal.

1.3.2 Imaging in Prostate Cancer

There are many imaging techniques currently in use for detecting and monitoring prostate cancer. MRI and ultrasound are used by many institutions in detecting the primary tumor upon suspicion of prostate cancer. In identifying spreading to surrounding lymph nodes, however, neither these diagnostics nor CT have proven reliable in staging, due to the lack of strong correlation between nodal metastasis and visible enlargement[36,37]. Utilizing PET to image primary prostate tumors also presents a problem, as kidneys very often filter out any foreign molecules. These filtered radiolabeled imaging probes subsequently accumulate in the bladder and block view of the prostate gland and pelvic lymph nodes.

Although effectively unable to identify primary site tumors, 2-FDG PET has proven useful in identifying metastasis of prostate cancer to both soft tissue and bone, but is not as sensitive to detecting bone metastasis as bone scintigraphy, with a sensitivity of only 65%[38].

Figure 6: 2-FDG PET scan[83] shows large signal in bladder, due to kidney functions. High signal in bladder makes imaging with PET impossible around bladder and surrounding tissue. Due to the proximity of the prostate to the bladder, PET imaging is typically useless in identifying primary site tumors.

Other PET imaging probes have also been tested for potential benefits for prostate cancer imaging. Since acetate is often utilized by cells to synthesize lipids, a process often amplified in cancer cells, C-11 labeled acetate has been tested as a potential PET probe. A recent study in 22 prostate cancer patients using C-11 acetate for PET showed marked improvement over 2-FDG PET, with a sensitivity of 100% in diagnosing primary tumors and lymph node metastases, as well as correctly identifying 6 of the 7 bone metastases. 2-FDG PET, in contrast,

Figure 7: PET molecular imaging probes for cancer are developed to take advantage of cellular processes or proteins that are typically amplified in cancerous transformations, such as cellular replication or lipid synthesis. (A) [C-11] Acetate is utilized for PET imaging with the goal of identifying increased fatty acid synthesis. (B) [C-11] or [F-18] Choline is utilized with the goal of identifying increased phospholipid synthesis. While both of these imaging probes have met with some success in imaging, both metabolites are involved in multiple cellular processes with several potential rate limiting steps, and may not be as reliable as hoped.

had a sensitivity of 83% diagnosing primary tumors, 40% diagnosing lymph node metastases, and

57% diagnosing bone metastases[39].

Choline is used as a precursor for the production of phospholipids in the cell, an

important part in cell proliferation and oncogenic transformation, and changes in choline

metabolism have been found in cancerous transformations[40,41]. [F-18] Choline (FCH) has been

combined with CT scans to identify locations of sites of metastasis in patients with prostate

cancer relapse, but is not useful in initial diagnosis due to its inability to distinguish between

cancerous tumors and benign prostate hyperplasia. Doctors must therefore first rely on PSA

levels as an indicator of potential relapse, and only after suspicious levels of PSA are detected use

PET scans to identify potential sites of relapse[36]. At the present time, [C-11]-choline PET/CT is not

recommended in the primary setting but may be utilized in clinically suspected prostate cancer

with repeatedly negative prostate biopsies, in preparation of a focused re-biopsy. Promising

results have been obtained for the use of PET and PET/CT with [C-11] and [F-18]-labeled choline

analogs in patients with biochemical recurrence. The detection rate of choline PET and PET/CT for

local, regional, and distant recurrence in patients with a biochemical recurrence shows a linear

correlation with PSA value at the time of imaging and reaches about 75% in patients with PSA > 3 ng/ml. Even at PSA values below 1 ng/ml, the recurrence can be diagnosed with choline PET/CT in approximately one-third of the patients[42]. A study specifically on lymph node staging for prostate cancer with [^{11}C]-choline showed a sensitivity of 80% and a specificity of 96%[37].

Further PET imaging probes have also met with minimal success. One molecule designed to measure testosterone uptake, 16-beta-[F-18]-fluoro-5-alpha-dihydrotestosterone (18F-FDHT PET) was compared with 2-FDG in a study involving 7 patients. 18F-FDHT PET showed a sensitivity of 77% in identifying tumor lesions in relapsed cancer, while 2-FDG PET showed a sensitivity of 97%. Out of the 7 patients, the 18F-FDHT PET only identified all detected lesions in 2 patients[43]. Together, these results are somewhat discouraging. While treatments for prostate cancer have worked well, accurate and cost effective diagnosis remain elusive in managing patient care.

1.3.3 Advantages and Assumptions of 2-FDG PET in Cancer

Out of each of these imaging methods available, PET offers the unique advantage of functional metabolic imaging. This allows the oncologist to identify not just the presence of the cancer, but also potentially estimate how aggressive the tumor is and how well it is responding to treatment. In particular, identifying any function unique to cancer, such as increased glycolytic metabolism, can give researchers insight into how tumors develop, and can direct work towards potential treatments. Much work has been done in measuring gene and protein expression in tumor samples with the hopes of developing treatments, but the reality is that even if a gene or protein is being expressed, it doesn't necessarily mean the protein is actually active and functioning in the cell, or that it is equally active throughout the entire tumor. Functional imaging allows researcher to skip this level of uncertainty, and directly measure activity.
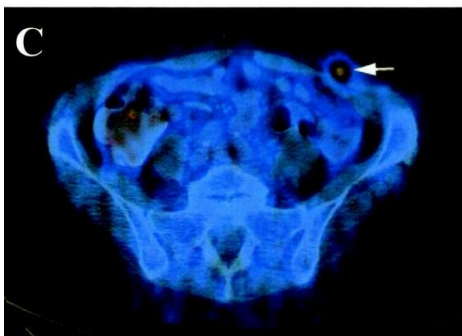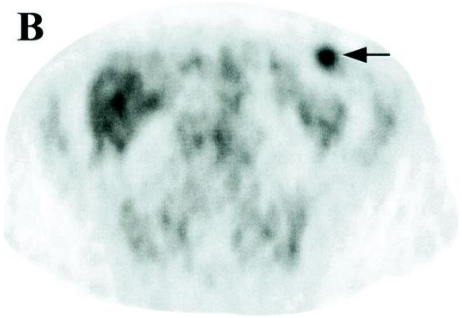
Figure 8: Combination of a CT scan (A) and a 2-FDG PET scan (B) into a PET/CT image (C). Arrow indicates presence of pancreatic cancer tumor[33].

For decades now, 2-FDG and [C-14]2DG have been used to quantify glucose metabolism *in vivo*, with 2-FDG being used both in humans and animals and [C-14]2DG limited only to animals. This metabolic rate has been quantified by utilizing a set of assumptions in measuring glucose uptake. The first is that glucose, 2-FDG, and 2DG are all taken up by the same set of transporters, thus compete with each other transporting back and forth between the blood and tissues, and also compete for hexokinase phosphorylation. The second is that 2-FDG and 2DG remain trapped within tissues once phosphorylation occurs, and are not metabolized further. The third is that the tissue being measured is homogeneous with respect to blood flow, metabolite concentration, and enzymatic activity. The fourth is that metabolite concentrations and metabolic flux remains roughly constant during the period of measurement. The fifth is that glucose, 2-FDG, and 2DG are perfectly mixed in blood and tissue, rather than being segregated into different pools. The sixth is that 2-FDG and 2DG and their respective phosphorylated products are present in trace amounts relative to the concentration of natural metabolites. The seventh is that the metabolite concentration in the capillaries is roughly equal to that of the arteries. The last assumption is that the contribution of radioactive signal in the

blood volume of the measured tissue is negligible relative to the amount of signal taken up by the tissue[44].

Interestingly, research over the past few decades has demonstrated that not all of the assumptions that have gone into 2-FDG PET imaging have been correct. While 2-FDG had been historically assumed to indicate total glucose transport, testing of SGLT specificity in the decades after their discovery revealed that sodium glucose transporters don't recognize either 2-FDG or 2DG. SGLTs, which transport glucose with significantly lower reversibility than GLUTs, are found in many tissues[45], forcing us to change our assumptions regarding 2-FDG PET imaging. In any tissue displaying significant SGLT activity, net transport of glucose through GLUTs as indicated by 2-FDG uptake is not necessarily equal to the rate of internal glucose phosphorylation. This has very significant implications in cancer imaging, as it is entirely possible for cancer cells with higher SGLT activity than GLUT activity to have high glucose consumption yet not present with high 2-FDG retention. From a perspective of tumor biology, SGLT proteins are a highly attractive option for glucose uptake, as poor blood vessel formation likely results in tumor regions that have less access to glucose. As passive glucose transporters rely on concentration gradients to
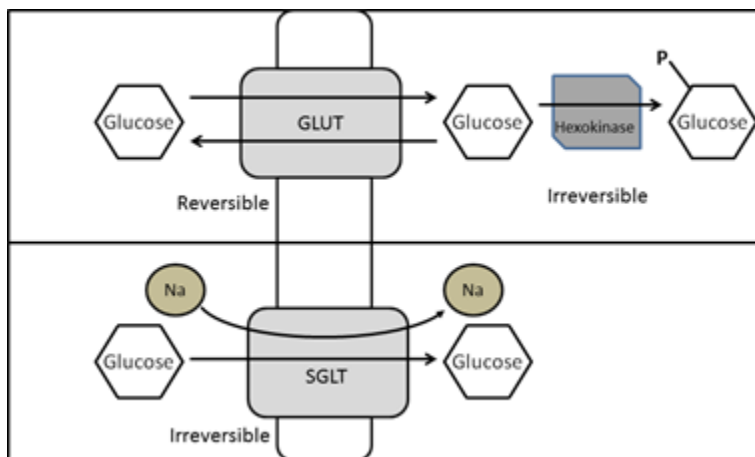
Figure 9: Unlike passive glucose transporters, which use a glucose gradient to facilitate glucose transport, SGLTs use a sodium gradient to transport glucose almost irreversibly. The traditional GLUT molecular imaging probe, 2-FDG, is not recognized by SGLT, and thus is not a complete indicator of total glucose metabolic rate. PET molecular imaging probes targeting SGLTs have the advantage of utilizing an initial step that is effectively irreversible, rather than relying on a downstream irreversible step, to capture radioisotope for generating signal.

transport glucose, low glucose levels can hinder glucose uptake.   Active transporters could

potentially rectify the problem of poor glucose supply by transporting glucose at high rates even

under low concentration conditions. If this is the case, utilizing molecular imaging probes that can

measure SGLT activity will be essential for accurately measuring glucose metabolism for cancers

that are increasing glucose uptake through SGLTs, rather than GLUTs.

1.4 Project Goals

Recent work has started to implicate sodium glucose transporters as contributors to cancer cell biology. Many cancerous tissues have been found to express SGLT protein and mRNA at much higher levels than normal tissue, and several cancer cell lines have been tested for SGLT activity *in vitro*. To date, however, there is no direct evidence of SGLT activity *in vivo*. If it can be established that SGLTs do play a critical role in cancer glucose utilization, they could become the perfect intersection between metabolic imaging and treatments directed toward cancer metabolism. This project will be the first effort directed at confirming the activity of sodium glucose transporters in live tumors, using the SGLT specific Me-4FDG for PET imaging.

Our first goal was to use Me-4FDG to image tumors in mouse xenograft models, allowing us to determine whether or not the SGLTs detected in immunohistochemistry and mRNA experiments are functionally active. We first tested several cell lines from cancers that were suspected of having SGLT expression to confirm SGLT activity *in vitro*, and then used those cell lines to generate the xenograft models. Our second goal was to continue the testing of SGLT activity in humans, by measuring Me-4FDG uptake in fresh, living tumor samples recently removed from patients with cancers that are suspected of having SGLT expression. If successful, these results would establish that Me-4FDG can be used to measure SGLT activity in cancer patients as a novel molecular imaging probe, and can also direct future therapeutic trials directed toward inhibiting SGLT function in tumors. Since sodium glucose transporters haven't been shown to be vital for survival in humans (with several SGLT2 inhibitors already in clinical trials for diabetes treatment, showing little or no side effects[46]), establishing SGLT activity in tumors will open the door to try some of these developed inhibitors for cancer treatment. These results will also open up a variety of other potential opportunities examining relationships between SGLT

activity and other aspects of tumors biology, such as regulator protein expression and patient survival.   If indeed SGLTs are active in cancer, it raises many interesting questions as to why cancer cells might choose to utilize active transporters, which require energy to use, when passive transporters are readily available.

2 Review of Sodium Glucose Transporters in Cancer

The existence and characteristics of sodium glucose transporters first started being proposed and tested in the 1960's. Early results identified the presence of sodium/glucose cotransporters, utilizing the energy from a sodium concentration gradient as the driving force behind active glucose transport in the intestinal brush-border membrane. Since then, SGLTs have been found highly active in both the kidneys and intestines, playing integral roles both in absorbing glucose from food and recycling glucose that has been filtered out through the kidneys[45]. For this reason, SGLTs have become a target for diabetes treatment, with the objective of lowering blood sugar levels in patients by inhibiting kidney SGLT activity[47]. SGLT mRNA expression has also been observed in a variety of other human tissues and organs, including brain, liver, thyroid, muscle, trachea, testis, lung, pancreas, prostate, and uterus, with functions ranging from glucose transport to glucose sensing, water transport, and even urea transport[45]. Recent work has also identified the functional activity of SGLTs in rat brains.[48,49]
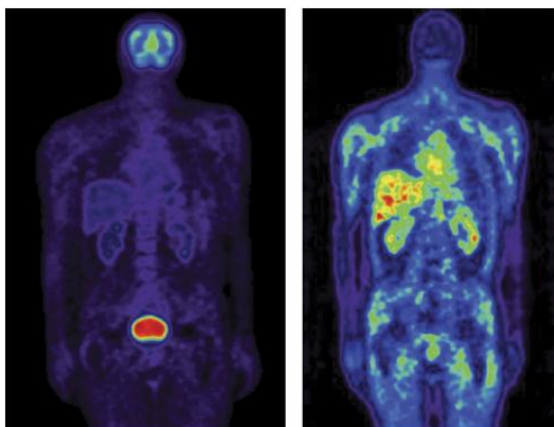
Figure 10: PET scans of 64-yr-old male using 2-FDG (left) and Me-4FDG (right). Scan shows significantly different biodistribution, with a large fraction of 2-FDG accumulating in the bladder[45]

Extensive work has been done in identifying substrate specificities and transport capacities of the various SGLT proteins discovered[45]. Currently, there are 6 known SGLTs, each with different properties. SGLT1 is recognized as a low capacity transporter with very high affinity toward glucose (K_m of 0.5mM), while SGLT2 is recognized as a higher capacity transporter with lower affinity toward glucose

(K_m of 5mM). Beyond glucose, SGLT1 also has affinity for galactose (K_m of 1mM) and various other glucose analogs not recognized by other SGLTs. SGLT3 is recognized as a glucose sensor, rather than dedicated glucose transporter. SGLT3 activity is highly sensitive to the concentration of glucose (with a K_m of 21mM), and the sodium that is transported in response to glucose is used as a signal to the cell, measuring extracellular glucose concentration[50]. SGLT4 has been found to have high affinity for mannose, with a K_m of 0.15mM, but is also capable of transporting glucose. SGLT5 was recently found to be expressed exclusively in the kidneys, capable of transporting multiple monosaccharides, with highest affinity for mannose and fructose[51]. SGLT6 is reported to be a transporter of myo-inositol, found in the brain and intestine[52]. The most widely effective SGLT inhibitor is phlorizin, demonstrating extremely low $K_{0.5}$ values for SGLTs, while at the same time unrecognized by GLUTs. A common inhibitor used specifically for SGLT2 is dapagliflozin (dapa), which has a significantly higher affinity for SGLT2 than SGLT1[45].

Both glucose analogs Me-4FDG and [C-14]methyl-alpha-D-glucopyranoside (αMDG) are selectively utilized by SGLTs, rather than GLUTs[45]. This selectivity gives it a drastically different distribution in the human body. Since SGLTs are highly active in the kidneys for recycling glucose, very little Me-4FDG builds up in the bladder. Likewise, Me-4FDG doesn't pass through the blood-brain barrier, since only GLUTs are active at the barrier, leaving no signal in the brain. Instead, stronger signal is seen in the muscles, liver, and kidneys. Another glucose analog, 4-fluorodeoxy-D-glucose (4-FDG) has been found to be transported by both SGLT1 and by GLUTs, but not other SGLTs. Unlike 2-FDG, 4-FDG is not phosphorylated by hexokinase, limiting the potential for it to accumulate in tumors that have high activity of reversible GLUTs. Since Me-4FDG and αMDG are solely transported through fairly irreversible SGLTs, they don't require phosphorylation to

accumulate in tissue, and as they are recognized by a wider range of SGLTs, can be used to effectively measure SGLT activity with greater versatility.

SGLTs have been observed in some cancers previously. SGLT1 protein expression has been observed in colorectal, head and neck, prostate, ovarian, cervical, and pancreatic cancer tumors, while SGLT2 mRNA expression has been observed in colorectal, gastrointestinal, head and neck, kidney, chondrosarcoma, and leukemia tumors. In addition, SGLT1 and SGLT2 mRNA expression has also been detected in lung cancer tumors[45]. Until recently, there has been no antibody for measuring SGLT protein expression other than SGLT1, so little work has been done on other SGLTs. Some initial reports have suggested that SGLTs may be essential for cancer cells to survive in low glucose environments, and have also started connecting SGLT activity to various regulators of cellular activity. There have also been a handful of experiments testing SGLT inhibitors such as phlorizin as cancer growth inhibitors both *in vitro* and *in vivo*, finding that phlorizin can reduce cancer growth rates[53]. If these links prove to be valid, it could potentially open up new doors of opportunity for diagnosing and treating several types of cancer.

2.1 Sodium Glucose Transporters in Prostate Cancer
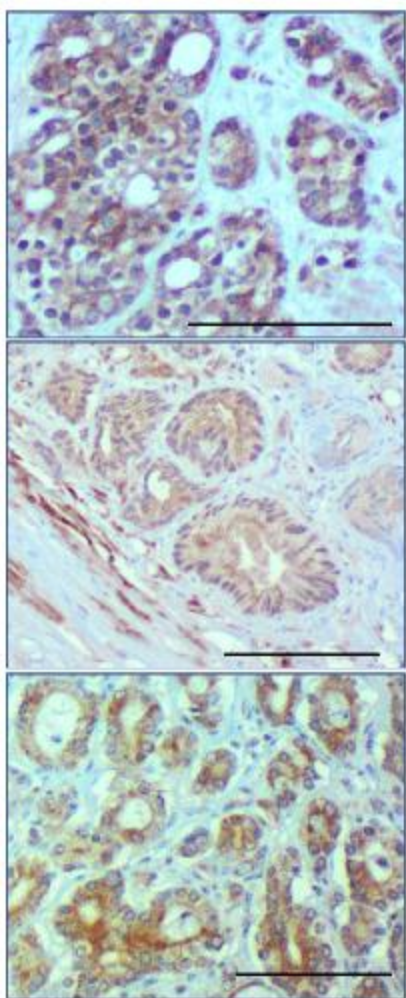
Figure 11: SGLT1 Protein staining in prostate cancer tissue samples[54]

Prostate cancer has been tested recently for evidence of SGLT expression. Antibodies generated from rabbits targeting amino acids 563-576 and 588-604 were used to examine SGLT1 protein expression in normal prostate, benign prostatic hyperplasia, prostatic intraepithelial neoplasia, and prostate cancer tissue samples. Immunohistochemistry analysis of the different tissue types showed marked increase in SGLT1 expression in the 44 prostate cancer samples tested over the 3 normal prostate tissue samples. Tests on other diseased prostate tissue also showed elevated SGLT1 expression, but to a less extent than prostate cancer samples[54].

In other results published by the same group, protein expression level data suggested that EGFR had the effect of stabilizing SGLT on the cellular membrane, allowing cells to take up glucose even when the concentration of available glucose is low. Decreasing EGFR levels caused increased rate of degradation of SGLT, causing cell death due to starvation in low glucose conditions. The loss of SGLT seemed to be due to protein degradation when EGFR is reduced in expression, or when the extracellular domain of the EGFR protein was removed. Coprecipitation experiments revealed EGFR and SGLT binding via the ECD of EGFR, an interaction that was lost when the domain was removed[55].

A subsequent publication by the same group tested EGFR and SGLT inhibition in prostate cancer cell lines PC-3 and LNCaP, and concluded that inhibiting cell lines with both SGLT inhibitor phlorizin (50μM) and either EGFR inhibitor Gefitinib or Erlotinib (20μM) had an additive effect in inhibiting cancer growth *in vitro*, concluding that the inhibitory effect of SGLT inhibition functions independently of EGFR kinase inhibition[56]. The epidermal growth factor receptor is often found overexpressed or highly active in epithelial tumors, and is associated with poor prognosis[57].   As a result, many research groups have looked into the role of EGFR in cancer progression, as well as potential treatments targeting EGFR. With these interesting connections between SGLT and EGFR observed in both lung and prostate cancer, there is an increasing desire to identify what roles SGLT activity may play in cancer survival.

2.2 Sodium Glucose Transporters in Pancreatic Cancer

Interestingly, recent work has shown that high expression levels of SGLT correlate with high levels of Bcl-2 in pancreatic cancer. In 45 pancreatic cancer patients tested for both SGLT1 and Bcl-2 expression levels, the 17 patients that had positive Bcl-2 staining showed significantly
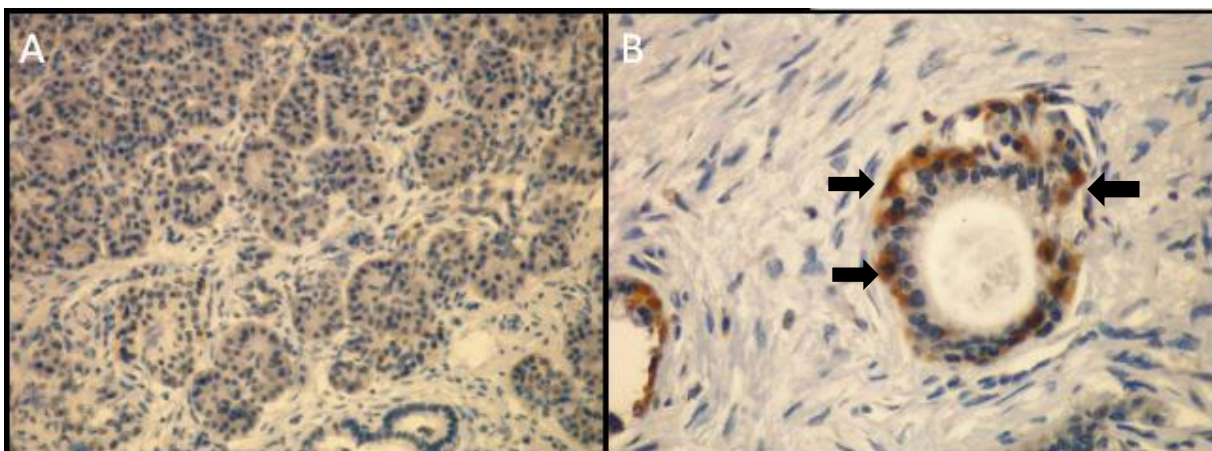
Figure 12: SGLT1 antibody staining of (A) normal pancreatic tissue and (B) excised pancreatic tumor sample. Normal pancreatic tissue shows no presence of SGLT1, while some pancreatic cancer tumor samples show presence of SGLT1, indicated by black arrows. SGLT1 staining correlated with Bcl-2 expression[58].

higher SGLT1 expression than the patients without[58]. Normal pancreatic tissue shows no presence of SGLT1 activity through either immunohistochemistry or PET imaging, indicating that the presence of SGLT1 would make a good target for imaging pancreatic cancer, and have the benefit of possibly providing information on patients that would benefit from therapies targeting Bcl-2. Since Bcl-2 plays an important role in the cell as an apoptotic regulator protein, forming heterodimers with other members of the Bcl-2 homolog family[59,60], and inhibitors of Bcl-2 are already in clinical trials for certain types of cancers[61–64], establishing connections between Bcl-2 and SGLT could be highly beneficial.

2.3 Sodium Glucose Transporters in Ovarian Cancer

A recent analysis of pathological specimens from 178 patients with epithelial ovarian tumors looked at SGLT1 protein expression using immunohistochemistry in a variety of tumor samples. The immunohistochemistry found that not only was SGLT1 expression elevated in tumors compared with normal tissue, higher SGLT1 expression correlated with increased tumor grade and poorer prognosis. While 0% of the normal ovarian tissue demonstrated high SGLT1 expression, 10% of the cystadenomas, 11.5% of the borderline tumors, and 39.7% of the invasive carcinomas demonstrated high expression[65]. While SGLT1 expression was clearly not a universal characteristic of ovarian cancers, the observation that SGLT1 expression tended to correlate with increased aggressiveness of the tumor strongly suggests that SGLT1 plays a role in growth and survival for some cases.

2.4 Sodium Glucose Transporters in Colon Cancer

Colorectal tumors and cell lines have both been tested for SGLT expression. The first tests in colorectal cancers were in the cell lines HT-29-D4 and Caco-2, identifying both SGLT1

expression with immunocytochemistry as well as phlorizin sensitive αMDG uptake *in vitro*[66,67].

While neither of these tests explored any potential survival benefit offered via SGLT activity, some of the tests did show that there were cases in which relative contribution of either SGLT or GLUT glucose uptake patterns were inversely proportional to each other, opening up the possibility that one mechanism may be compensating for a lack in the other. A more recent analysis tested for SGLT1 and EGFR expression in 85 formalin fixed, paraffin-embedded colorectal cancer pathology specimens compared with 28 normal tissue samples, finding that SGLT1 expression correlated with higher clinical stage of cancer while normal tissue was absent of staining[68]. Comparing EGFR expression to SGLT1, the group found no correlation between EGFR and SGLT1.

2.5 Sodium Glucose Transporters in Lung Cancer

In a lung adenocarcinoma cell line, increased SGLT activity was shown to help cells survive in response to irradiation *in vitro*, mediated by epidermal growth factor receptor (EGFR) kinase activity[69]. The A549 cell line was irradiated with x-rays and tested for phlorizin sensitive glucose uptake. In the patch clamp and [^{3}H]-glucose tests, sodium dependent glucose uptake was found to be significantly increased in response to radiation *in vitro*. In contrast, cells inhibited with phlorizin or erlotinib to stop either SGLT or EFGR activity showed no increased glucose uptake, and had poorer survival response to radiation than cells that were not treated with inhibitors. Another analysis of 96 autopsy samples from 35 patients tested for mRNA expression of both SGLT1 and SGLT2 found the SGLT2 expression was elevated in metastatic regions of lung cancer in either lymph nodes or liver when compared with normal tissue or primary site tumors. In

contrast, no difference in expression of SGLT1 was observed in either normal, primary site, or metastasized tumor site tissues[70].

2.6 Sodium Glucose Transporters in Head and Neck Cancer

SGLT1 expression has been confirmed both in head and neck cancer cell lines as well as tumor samples. Thirty six short term head, neck, and shoulder cancer cell lines cultivated from cancer tumors were tested for RNA expression of both SGLT1 and SGLT2. RT-PCR showed mRNA expression of SGLT1 in 17 out of the 36 cell lines, with no expression of SGLT2. Immunohistochemistry staining in 30 fresh, flash frozen tumor samples showed heterogeneous SGLT1 staining in 27 specimens, always limited to differentiated tumor areas[71]. The authors also observed that cell lines created from tumors with very little SGLT1 staining also tended to have no SGLT1 mRNA, speculating that the lack of RNA expression might be due to differences in the *in vitro* environment. While there was no testing for confirmation of SGLT activity in either the cancer tumors or cell lines, the results did suggest that SGLT1 expression had the potential to be used as a differentiation marker.

Recent tests on oral cancer tumor samples and cell lines have also shown correlations between SGLT1 expression and EGFR. Tests on 6 different cell lines developed from squamous cell carcinoma showed each cell line expressing both EGFR and SGLT1 *in vitro*. Immunohistochemistry of tumor tissue samples from 52 patients tested also showed significant correlation between EGFR expression and SGLT1 expression. The expression of EGFR and SGLT1 also was found to correlate with tumor differentiation, with the less differentiated cancer tissues expressing higher levels of EGFR and SGLT1[72].

2.7 Sodium Glucose Transporters in Cervical Cancer

Sodium glucose transporters have also been recently observed in cervical cancers. In a recent survey of tumor samples from 254 patients of varying age, tumor grade, and stage, SGLT1 immunohistochemistry staining showed some level of SGLT1 expression in 40% of the samples, with adenoma benign tumors showing no SGLT1 expression. In addition, analysis of tumor protein expression found that tumors with stronger staining for SGLT1 also tended to have stronger staining for MAP17, a membrane protein associated with many cancers. Analyzing individual tumors showed similar results, with regions expressing higher SGLT1 also expressing higher MAP17. Protein expression also correlated with overall survival, with patients demonstrating higher SGLT1 and MAP17 staining also having a more favorable prognosis. Patients with lower SGLT1 and MAP17 staining tended to have poorer survival rates[73].

In addition to testing tumor samples for SGLT1 and MAP17 expression, the researchers also examined the effect of MAP17 expression on SGLT1 activity. The cervical cancer cell line HeLa was tested for SGLT1 protein expression as well as glucose consumption in response to overexpression of MAP17 *in vitro*. It was found that HeLa cells transformed to overexpress MAP17 also had elevated SGLT1 levels and glucose consumption, as tested by [2–3H] glucose uptake. The increased glucose uptake rate was negated by the SGLT inhibitor phlorizin, suggesting that the increase in SGLT1 expression resulted in the increased glucose consumption.

3 Activity of Sodium Glucose Transporters in Animal Models

3.1 Introduction

With mounting evidence that SGLTs play a significant role in at least some cancers, the idea of using Me-4FDG for PET imaging is becoming an increasingly attractive prospect. Although multiple groups have reported elevated SGLT expression in cancers, as well as signs of survival benefit *in vitro* connected to SGLT expression, to date there have been no experiments conducted to confirm SGLT activity *in vivo*. In order to confirm this, we first established mice xenograft models to test for Me-4FDG uptake, indicating SGLT activity. Thus our first goal was identifying ideal cell lines to use for animal models, and from there establishing the animal model to test for *in vivo* SGLT activity with Me-4FDG PET imaging. Observing Me-4FDG uptake in mice xenografts would then give us further justification to continue testing in humans.

As discussed earlier, several cell lines and tumor pathology samples have already been tested for SGLT protein or mRNA expression. Using these initial results as starting points, we first selected cell lines to test for SGLT activity, and then used the most promising lines to establish mice xenografts. Our expectation was that cell lines that had high Me-4FDG uptake *in vitro* would also have high Me-4FDG uptake *in vivo*, allowing us to use Me-4FDG PET imaging to diagnose and characterize tumors. Confirmation of Me-4FDG uptake via PET imaging in this project would be the first data confirming SGLT activity in live tumors, and allow us to explore potential reasons for tumors to use active sodium glucose transporters rather than passive glucose transporters for glucose consumption. Evidence has been presented suggesting that sodium glucose transporters provide survival benefits to cancer in stressed or low glucose conditions[55,69], but none of those tests were conducted *in vivo*. These models would give us the ability to look for evidence of

survival advantages offered by SGLT activity, such as higher SGLT activity in tumor regions that have poor blood supply, or increased SGLT activity with lower blood sugar levels.

While testing the cell lines for Me-4FDG uptake, another option we explored was testing the connections to regulatory proteins previously reported, such as connections with EGFR that have been observed in lung and prostate cancer cell lines. Despite the pattern of upregulation of EGFR in many cancers, EGFR activity inhibitors such as gefitinib and erlotinib have had poor clinical trial performance, with only a small percentage of patients showing benefit[74]. Given evidence that EGFR can enhance cancer survival through SGLT activity, testing for effects of EGFR inhibition and SGLT inhibition on Me-4FDG uptake could give insight into guiding potential EGFR-based treatments.
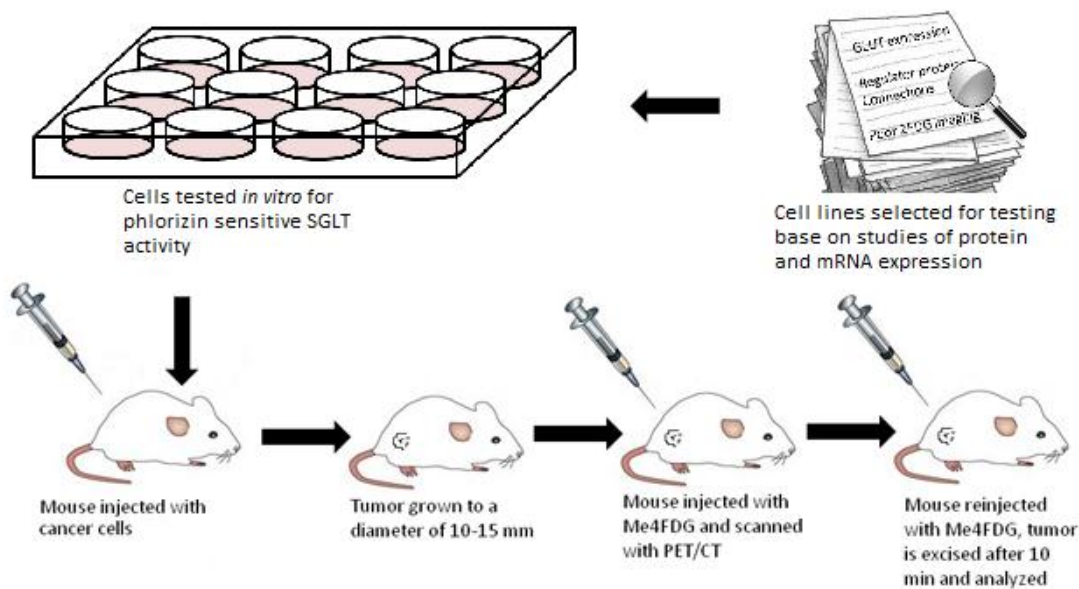
Figure 13: Methodology for establishing viability of Me-4FDG PET scan for selected cancers

3.2 Materials and Methods

3.2.1 Cell lines and reagents

Cancer cell lines AsPC-1(pancreatic), MiaPaCa-2(pancreatic), and BxPC-3(pancreatic) were obtained from American Type Culture Collection (ATCC). AsPC-1 and BxPC-3 cell lines were grown in RPMI 1640 media (ATCC) with 10% fetal bovine serum (FBS) added. MiaPaCa-2 cells were grown in DMEM media (ATCC) with 10% FBS and 2.5% horse serum added. All media contained 100 U/mL penicillin and 100 mg/L streptomycin.

C-14 labeled αMDG and C-14 labeled mannose were obtained from Moravek Biochemicals. Stock concentrations of αMDG were 2mM with a specific activity of 50Ci/mole, and stock concentrations of mannose were 1.8mM with a specific activity of 55.5Ci/mole. Ultimal Gold LSC-cocktail for scintillation counting was obtained from Perkin Elmer.

3.2.2 *In vitro* sodium glucose transporter activity

SGLT Activity Assay

SGLT activity was determined using radiolabeled αMDG uptake. Cells were grown in 12-well or 24-well plates until confluent. Media was removed and cells were washed three times with warm PBS buffer. 400μL (for 12-well plates) or 250μL (for 24-well plates) of PBS containing 50μM αMDG with a specific activity ranging between 10 and 40 Ci/mole was added to each well, and cells were incubated at 37°C for 30-60 minutes with or without phlorizin ranging in concentration from 10μM to 1mM. After incubation, media was removed and cells were again washed with chilled PBS three times. Cells were lysed with 0.1% Triton-X-100 in PBS and lysate was collected for each sample.

To test for sodium dependent uptake, grown cells were washed three times with either sodium chloride or choline chloride buffers containing either 150mM NaCl or 150mM choline chloride with 1mM $CaCl_2$, 1mM $MgCl_2$, and 10mM HEPES, titrated to pH 7.4, then incubated in either the sodium chloride or choline chloride solution containing 50µM [^{14}C]-αMDG with a specific activity of 10Ci/mole for 45 minutes with or without 100µM phlorizin. Cells were then washed and lysed as previously described.

Scintillation

Uptake of αMDG was calculated by measurement of radioactivity present in cell lysate recovered from SGLT activity assay. A fraction of the recovered lysate was mixed with 4mL of Ultima Gold LSC-cocktail in 10mL glass vials and vortexed to mix. Radioactivity of vials was measured using a Beckman LS-6500 Scintillation Counter, and then divided by total volume of lysate used. Vials containing 10uL of uptake solution of 50µM αMDG mixed in 4mL were used as the standard to calculate pmole of αMDG per count.

Bradford assay

Cellular protein was determined by Bradford assay. Bio Rad Protein Assay Dye Reagent Concentrate was diluted 5 fold in water to a final volume of 990µL. 10µL of lysate from cells disrupted with 0.1% Triton-X in PBS was thoroughly mixed with diluted reagent, and absorbance at 595nm was measured via spectrophotometer. BSA was dissolved in 0.1% Triton-X PBS at concentrations of 0.25mg/mL, 0.5mg/mL, and 1mg/mL to use as a standard.

3.2.3 Cell survival assay

Cells were seeded in 12-well plates in DMEM at 50k cells/well and grown for two days. After the two days of growth, cell media was replaced with 2.5mM glucose RPMI media containing with or without either 100μM phlorizin, cobalt chloride, or both. After two days, cells were trypsinized and centrifuged. Cells pellets were resuspended in 50μL PBS, and then mixed with an equal volume of trypan blue for staining. Cells were then counted on a hemocytometer, with dead cells staining blue and live cells transparent.

3.2.4 Animal xenografts

Immunodeficient Nod SCID gamma (NSG) mice were injected with $2x10^6$ cells from either PC-3 or AsPC-1 cancer cell lines. Mice were imaged using Me-4FDG microPET for 1 hour, then subsequently imaged by CT.

3.2.5 PET/CT scans

Animals with fully developed tumors were anesthetized and injected with 120-170μCi of either Me-4FDG or 2-FDG diluted in sterile saline solution. For Me-4FDG scans with SGLT2 inhibited, dapa was diluted in injection solution at a concentration of 1.0 mg/kg for most scans, with one mouse injected with 0.5mg/kg and one injected with 0.2mg/kg. Two other mice were injected with dapa 10 minutes before Me-4FDG injection, while one was injected with dapa 10 minutes after Me-4FDG injection.

PET scans were performed for one hour in either Siemens Inveon or Concord Microsystems Inc. Focus microPET scanners. CT scan was performed immediately afterward for 10 minutes in ImTek Inc. Microcat II CT scanner. Fused PET/CT scans were analyzed using AMIDE medical imaging data examiner. Regions of interest (ROIs) were drawn manually by two

independent researchers to eliminate potential bias. SUV of regions of interest was calculated by

dividing the total signal of ROI by the total volume of the ROI, then dividing by total injected signal

per gram of mouse weight. Total injected signal at each time point was calculated by multiplying

mean measured signal at each time point by total mouse volume and dividing by scanner cylinder

factor, rather than using the measured syringe injection dose before injection. This allowed us to

more accurately gauge the total injected, bioavailable dose.   Scans with significant increase

(>10%) in total inject signal over time (indicating poor injection with large buildup in the tail) were

not used for averaging time activity curves, as SUVs calculated for those scans aren't as reliable.

3.2.6 Autoradiography

After the Me-4FDG PET scan, mice were injected with 500-1000 µCi of additional Me-

4FDG and sacrificed after 10-30 minutes. Tumor was excised and flash frozen in Tissue-Tek O.C.T.

Compound for slicing. Embedded tissue was cut on a Leica CM3050S cryostat into slices 20

microns thick and mounted on glass slides for autoradiography and immunohistochemistry.

Autoradiography film was exposed to sliced tissue samples under dark conditions for 1

hour, and then analyzed in a Fujifilm BAS-5000 image reader. Tissue slides were subsequently

soaked in formalin solution for fixation to preserve for immunohistochemistry.

3.2.7 Immunohistochemistry

Tumor slices mounted on slides were fixed by soaking in 10% formalin for at least 10

minutes and left to dry overnight. Antigen retrieval was performed with 10mM citrate buffer, pH

6.0, at 95°C for 10-40 minutes. Slides were washed four times with PBS (standard wash 3

minutes, 5 minutes, 7 minutes, and 7 minutes) then incubated with 0.3% hydrogen peroxide for

30 minutes, then washed 4 times with PBS. Tissue slices were dried with vacuum line and

incubated for 30 minutes in blocking buffer (5% normal donkey serum and 0.1% sodium azide in PBS). Blocking buffer was removed and tissues were incubated overnight with primary antibody solution (5% normal donkey serum, 0.1% sodium azide, and primary antibody). Antibodies were diluted 1/100. Primary antibodies were purchased from Abcam (GLUT1, 15309; GLUT3, 15311). Human brain tissue was used as positive control for GLUT1 and GLUT3 expression.

Slides were washed the next day four times with PBS, gently dried with vacuum line, then incubated with secondary biotin-anti-rabbit antibody diluted 250-fold in PBS with 10% donkey serum for at least 1.5 hours. Slides were again washed four times with PBS, dried gently with vacuum line, and then incubated with ABC reagent for at least 1.5 hours. After final PBS washes, tissues were again dried and incubated with UREA hydrogen peroxide and DAB for 10 to 20 minutes, until antibody staining developed. For counterstain, slides were immersed in nanopure water, followed by 20 second immersion in 1:5 Harris hematoxylin diluted in nanopure water. Slides were then washed twice in nanopure water for 2 minutes each, followed by 2-3 second immersion in ammonium hydroxide solution, then an additional two washes in nanopure water for 2 minutes each. Tissues were dehydrated by serial immersion for 2 minutes each in 70% ethanol, 95% ethanol, 100% ethanol, xylenes, and xylenes.

3.3 Selection of Cell Lines

Our first milestone in determining tumor SGLT activity in animal models was identifying ideal starting cell lines. Since pancreatic, ovarian, and prostate cancers have stood out as often being very difficult to detect using conventional imaging techniques, we first selected different established cancer cell lines to test for SGLT activity in cell culture. The primary concern in this selection was identifying cell lines with significantly different phenotypes, with the goal of either finding a phenotype that correlated with SGLT activity or finding that SGLT activity remained independent of other characteristics of the cancer cell lines.

Three commonly used pancreatic cancer stains, AsPC-1, MiaPaCa-2, and BxPC-3, were selected based primarily on mRNA levels of GLUT1, with BxPC-3 showing high expression of GLUT1 relative to normal pancreas tissue and AsPC-1 and MiaPaCa-2 showing lower levels of GLUT1 mRNA[75], as indicated in Figure 14. We hypothesized that SGLT activity could compensate for a lack of increased GLUT expression in cancer cells, and that we would see an increase in SGLT activity in MiaPaCa-2 and AsPC-1 cells relative to BxPC-3 cells in culture.

Affy probe_set	Gene Name	Unigene Comment
X93036_at	FXYD3	FXYD domain-containing ion transport regulator 3
Y07604_at	NME4	non-metastatic cells 4, protein expressed in
U33632_at	KCNK1	potassium channel, subfamily K, member 1 (TWIK-1)
K03195_at	SLC2A1	solute carrier family 2 (facilitated glucose transporter), me
X57522_at	TAP1	transporter 1, ATP-binding cassette, sub-family B (MDR/TA

Figure 14: Microarray data of various pancreatic cancer cell lines, tumor samples, chronic pancreatitis samples, and normal pancreas tissue. GLUT1 mRNA expression (Gene Name SLC2A1) in BxPC-3, MiaPaCa-2, and MPanc-96 (cell line representative of ASPC-1[76] is shown relative to average expression. Both MiaPaCa-2 and MPanc-96 show no noticeable increase in GLUT1 expression, in contrast to BxPC-3.[75]

LNCaP, PC-3, and C4-2 prostate cancer cell lines are commonly used in studying prostate cancer. LNCaP cells are an androgen-dependent cell line that was derived from a lymph node metastasis and expresses both androgen receptor protein (AR) and prostate specific antigen

(PSA). In contrast, PC-3 cells are androgen-independent, expressing neither AR nor PSA, and were derived from a bone metastasis.[77,78] The C4-2 cell line was derived from the LNCaP line in castrated mice, showing the same AR and PSA expression, but with less androgen sensitivity.[79] These cell lines represent an ideal spectrum of prostate cancer, as LNCaP is typically used to model an indolent form of prostate cancer, while PC-3 cells are often used as the model of more aggressive cancer.

Conflicting reports have found prostate cancer tissue with higher GLUT mRNA expression as measured with mRNA hybridization, shown in Figure 15, but no increase in GLUT protein levels as detected with antibody immunohistochemistry[80]. This lack of consistency in passive glucose transport makes this cancer particularly appealing to test for active glucose transport. If the passive glucose transporters are not overexpressed in these cell lines, it would be reasonable to suspect that active glucose transporters could significantly contribute to glucose uptake. Utilizing these cell lines also gives the benefit of identifying potential differences in SGLT activity between cell lines of different aggressiveness.

Figure 15: Northern blot of GLUT1 mRNA expression in normal prostate tissue (NP), LNCaP, DU145, and PC-3 cancer cell lines. Results show higher GLUT1 expression in prostate cancer cell lines, despite conflicting reports that clinical prostate cancer specimens showed no increased GLUT1 protein levels when tested with immunohistochemistry.[80]

3.4 Initial Testing of SGLT Activity

3.4.1 SGLT activity in pancreatic cancer cell lines correlates with lower GLUT mRNA expression

SGLT activity was determined by uptake of αMDG. Cell cultures grown in well plates were incubated in the presence of C-14 labeled αMDG with or without phlorizin. Well plates with phlorizin were used as the background signal, since phlorizin completely inhibits SGLT activity, and the difference between the background signal and the signal without phlorizin was used to calculate the rate of αMDG uptake through SGLTs.
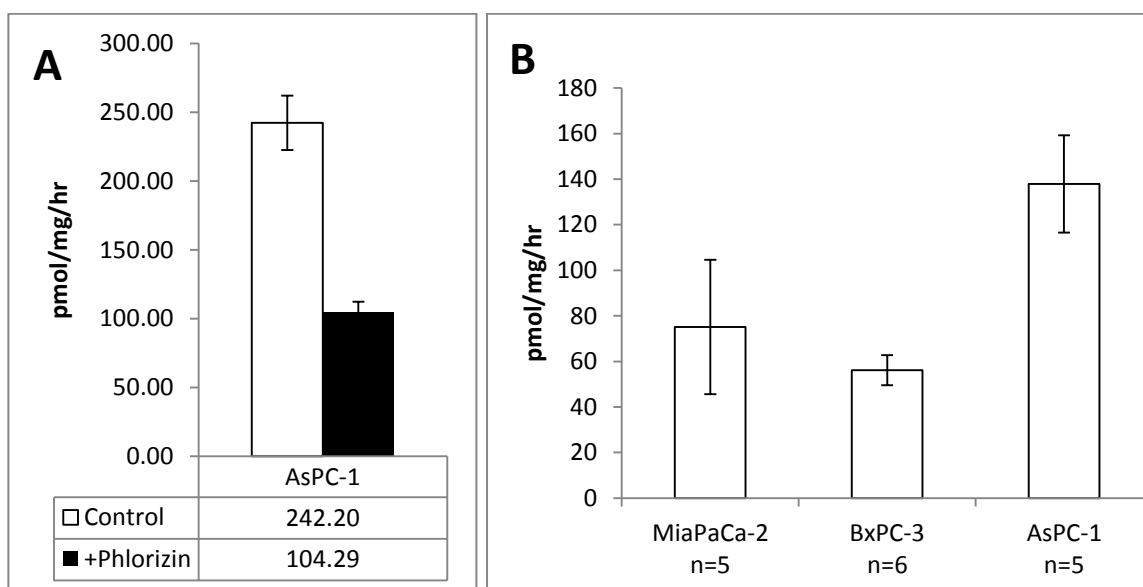
Figure 16: Phlorizin dependent αMDG uptake in MiaPaCa-2, BxPC-3, and AsPC-1 pancreatic cancer cell lines, measured in pmol/mg cell protein/hour. (A) Uptake of C-14-αMDG is measured with or without phlorizin in AsPC-1 cells. SGLT activity is calculated by subtracting the uptake in the presence of phlorizin from the uptake without phlorizin. (B) The SGLT activity of MiaPaCa-2, BxPC-3 and AsPC-1. Standard error used for error bars. As predicted, higher SGLT activity is observed in cell lines expressing lower GLUT mRNA.

Initial tests on pancreatic cancer cell lines MiaPaCa-2, AsPC-1, and BxPC-3, confirmed the initial hypothesis. As shown in Figure 16, BxPC-3 predictably showed minimal SGLT activity, while AsPC-1 demonstrated noticeable SGLT activity ranging between 100 and 180 pmol/mg protein/hr.

MiaPaCa-2 cells showed significant uptake, but extremely high variability. As a result, the AsPC-1 cell line was selected for further testing of SGLT activity.

3.4.2 SGLT active in PC-3 prostate cancer cell line

As shown in Figure 17, initial uptake tests on prostate cancer cell lines PC-3 and C4-2 revealed noticeably higher SGLT activity in the more aggressive PC-3 cell line and negligible activity in the C4-2 cell line. Tests on tolerance for glucose starvation conditions also revealed that PC-3 cell cultures were highly tolerant to glucose starvation, while both LNCaP and C4-2 cells were unable to recover from glucose deprivation. While PC-3 did demonstrate high variability in SGLT activity after multiple experiments, their SGLT activity was sufficient to also be chosen for subsequent cell line tests and animal xenografts.
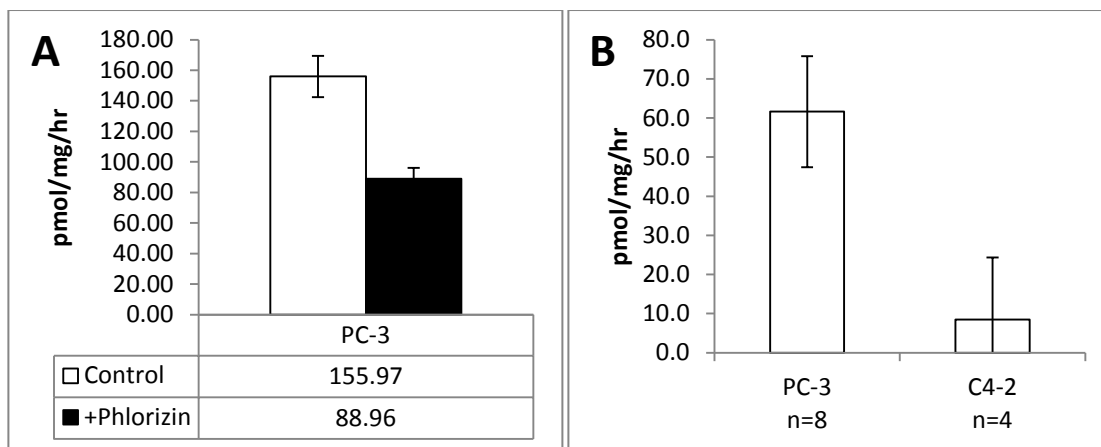
Figure 17: Phlorizin dependent αMDG uptake in PC-3 and C4-2 prostate cancer cell lines, measured in pmol/mg cell protein/hour. (A) Uptake of C-14-αMDG is measured with or without phlorizin in PC-3 cells. SGLT activity is calculated by subtracting the uptake in the presence of phlorizin from the uptake without phlorizin. (B) The SGLT activity of PC-3 and C4-2 cell lines. Standard error used for error bars. SGLT activity is present in PC-3, but with high variability. No SGLT activity observed in C4-2 cells.

3.4.3 Repeated tests unable to identify specific SGLT

We then conducted further experiments with the AsPC-1 and PC-3 cell lines to identify the specific SGLT responsible for the phlorizin inhibited uptake of αMDG. SGLT1 has high preference for galactose, with a measured K_m of 1mM (0.5mM for αMDG), while dapa acts as an inhibitor of SGLT2 with a $K_{0.5}$ of 0.001μM. To test for the activity of SGLT1 versus SGLT2 (the two most likely candidates for SGLT activity), we incubated AsPC-1 and PC-3 cells with αMDG in the presence of either phlorizin (100μM) to block all SGLT activity, dapa (10 μM) to block SGLT2 activity, or galactose (25mM)to block all SGLT1 activity, in order to identify the responsible transporter. As Figure 18 shows, neither galactose nor dapa caused a reduction in αMDG uptake in repeated experiments in either cell line. Phlorizin continued to significantly reduce αMDG uptake.
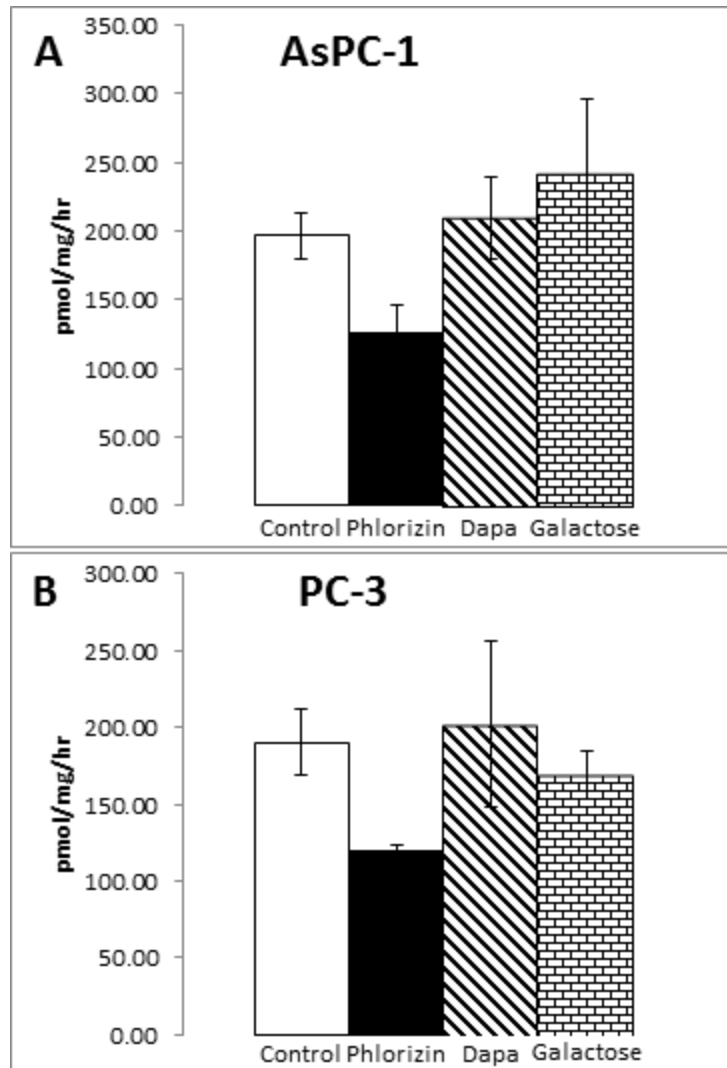
Figure 18: Inhibition of αMDG uptake in AsPC-1 (A) or PC-3 (B) cells with phlorizin, dapa, and galactose in cell culture to test for either SGLT1 or SGLT2 activity, n=6 for each condition. Results show no decrease in αMDG uptake in the presence of dapa or galactose, indicating phlorizin dependent uptake independent of SGLT1 or SGLT2.

This was particularly unexpected, as SGLT1 and SGLT2 were the most likely candidates for SGLT

activity in these cell lines. With these two candidates seeming unlikely, we continued to look for other likely SGLT candidates.

Another possible SGLT transporter to explore was SGLT4, which transports both glucose and mannose and is also inhibited by phlorizin. To test for the possibility of SGLT4 or 5 activity, we incubated AsPC cells with C14 labeled mannose, which isn't taken up by any of the other SGLT transporters. To eliminate uptake of the C-14-mannose through GLUTs, 10µM cytochalasin B was added to the uptake solution to inhibit GLUT activity. Shown in Figure 19, there was no difference in mannose uptake with or without phlorizin, indicating the absence of SGLT4 or SGLT5 activity. As a comparison, the experiment of αMDG uptake with or without phlorizin was repeated with cytochalasin B added. No decrease in SGLT dependent αMDG was observed. As a similar test in PC-3 cells, cells were incubated with αMDG with or without mannose to inhibit uptake. Initial tests revealed no significant difference in αMDG (data not shown) likewise indicating a lack of SGLT4 or SGLT5 activity.
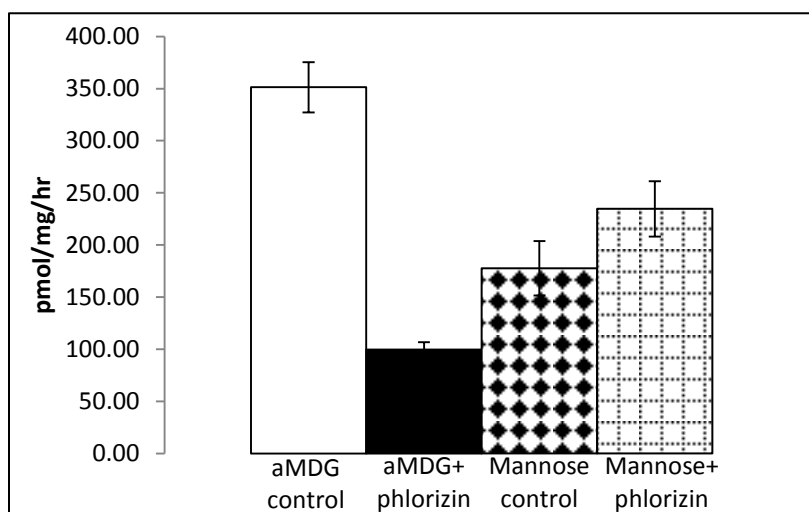
Figure 19: Mannose uptake in AsPC-1 cell line to test for SGLT4 activity, n=6 for each condition. Mannose uptake rate was compared with the uptake rate of αMDG in the presence of GLUT inhibitor cytochalasin B. Results show no phlorizin dependent uptake of mannose, indicating lack of SGLT4 activity.

These results left us with several possibilities with regard to the nature of the SGLT activity present in the cell lines. One possibility was that we were observing the activity of an unknown, phlorizin sensitive SGLT. Another was that multiple SGLTs were present and active, compensating for the inhibition of each other. Yet another was that the concentrations or conditions of inhibitors used to test for individual SGLTs were insufficient to completely inhibit uptake. Rather than continuing to try to identify these unknown SGLTs, we instead turned our attention to confirming that the activity we were seeing was indeed characteristic of SGLTs, sensitive to phlorizin and sodium.

3.4.4 Confirming sodium glucose transporter characteristics

We first tested phlorizin sensitivity of the PC-3 and AsPC-1 cell line SGLT activity, to confirm we were actually measuring sodium, glucose transporter activity. As shown in Figure 20, increasing phlorizin to a concentration of 1mM continued to reduce activity in the PC-3 line, while between 10 and 100uM phlorizin was sufficient to inhibit all SGLT activity in AsPC-1.
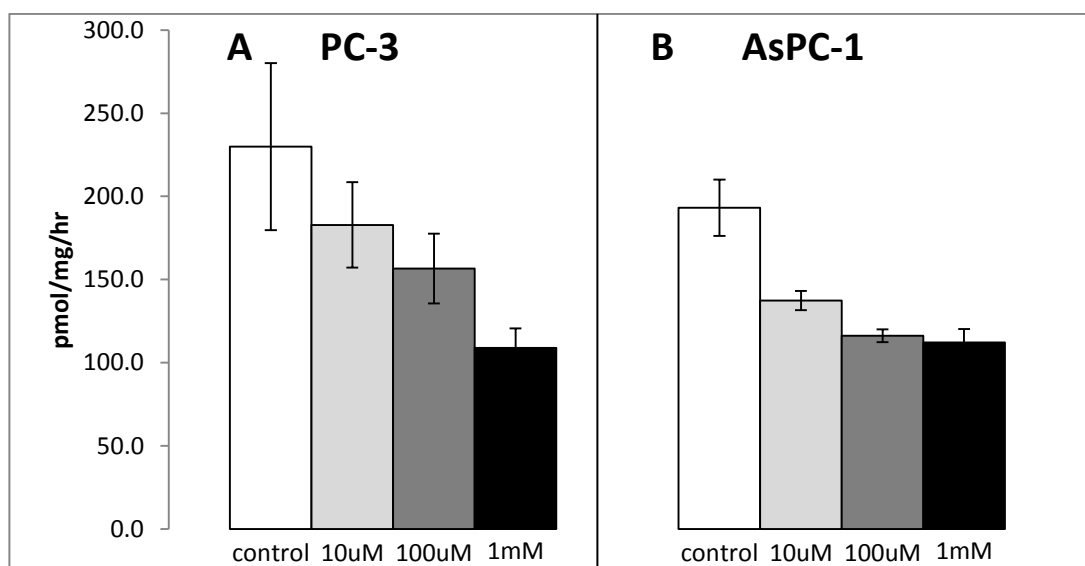
Figure 20: Phlorizin sensitivity of PC-3 (A) and AsPC-1 (B) cell line SGLT activity, n=3 for each. AsPC-1 shows slightly higher sensitivity to phlorizin inhibition, with 10uM being almost sufficient to completely eliminate all αMDG uptake.

To test for sodium dependence, AsPC-1 cells were incubated with αMDG in either a sodium chloride or choline chloride solution. As shown Figure 21, all phlorizin dependent uptake was completely eliminated with the removal of sodium in the uptake solution, indicating complete dependence on sodium for activity. Retesting phlorizin inhibition under these conditions, we also found that the cell lines remained highly sensitive to phlorizin, with even 1μM phlorizin sufficient to significantly inhibit uptake. These tests confirmed that αMDG uptake is through some sodium glucose transporter active in these cell lines, although the identity of the specific transporter remained elusive.

	sodium buffer	sodium buffer 1uMphlorizin	sodium buffer 100uMphlorizin	choline buffer	choline buffer 100uMphlorizin
	410.1	290.0	204.5	179.5	173.4
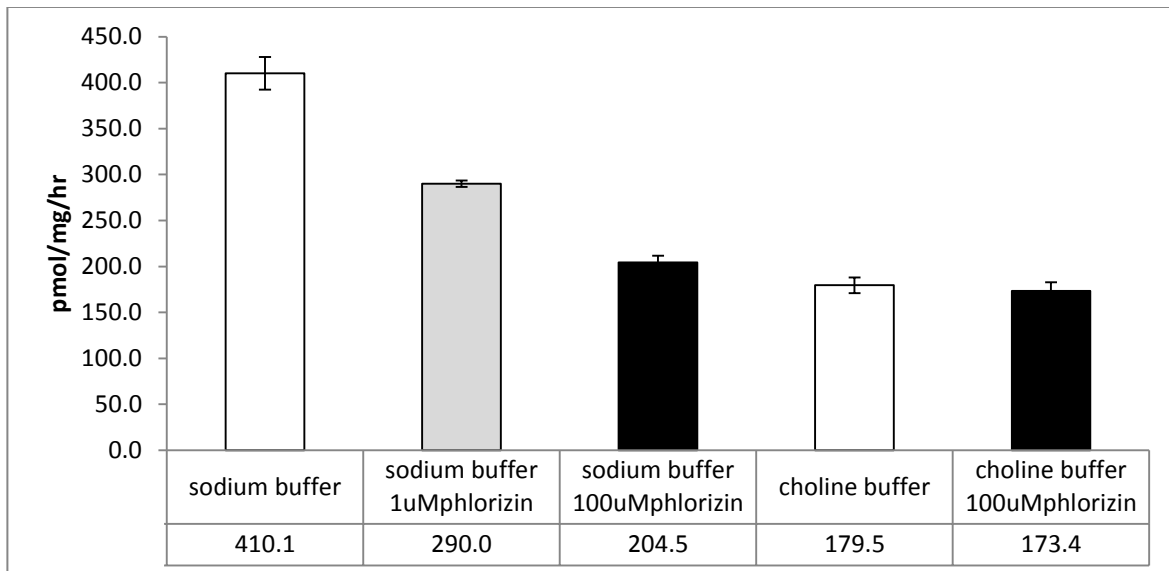
Figure 21: Testing for sodium dependent glucose uptake in AsPC-1 cell line in either sodium chloride or choline chloride buffers, n=4 for each condition. Uptake was highly sensitive to phlorizin inhibition, with 1uM phlorizin being sufficient to cut phlorizin dependent uptake in sodium buffer in half. Removal of sodium in buffer completely eliminates all phlorizin sensitive glucose uptake.

3.5 Cell survival assays

Sodium glucose transporters have been implicated in survival benefits in both prostate and lung cancer cells in low glucose stress conditions, so we wanted to see if there may be any response to low glucose conditions, as well as test for any survival benefit from SGLTs.

3.5.1 Glucose starvation slightly increases measured SGLT activity

Since we reasoned that SGLTs might be beneficial to cancer tumors due to their ability to continue taking up glucose in low glucose concentrations, allowing tumors to survive in an environment with poor blood supplies, we tested the response of PC-3 SGLT activity to varying concentrations of glucose. Cell cultures were grown for three days in either 25mM (high), 11.5mM (medium), or 2.5mM (low) glucose, and tested for αMDG uptake. As expected there was a very slight but statistically significant decrease in SGLT activity as glucose concentration increased, indicating the possibility that the cancer cells were responding to low glucose environments by increasing active transport of glucose.

	Low Glucose	Medium Glucose	High Glucose
□ control	101.8	94.7	87.0
■ +phlorizin	70.4	64.3	70.0
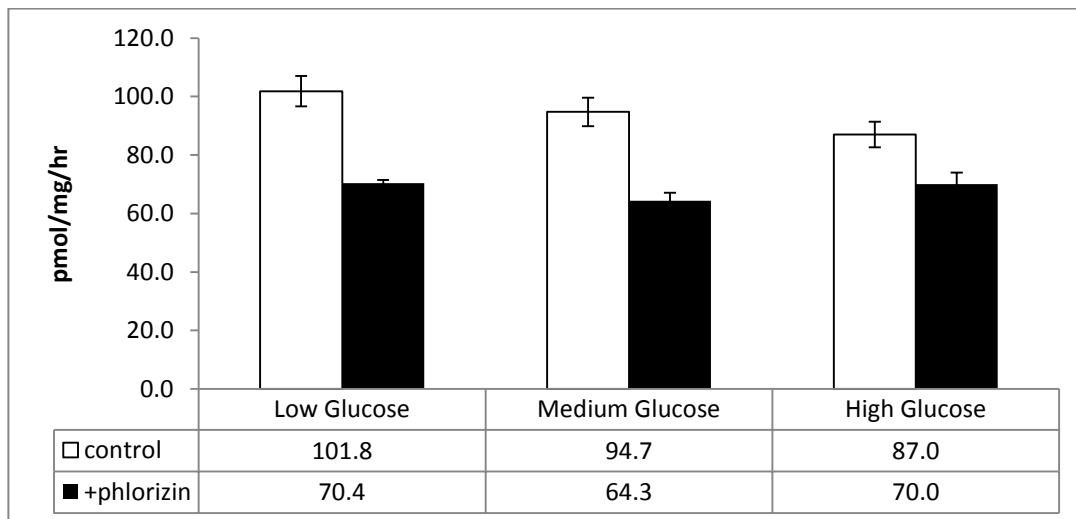
Figure 22: Uptake of αMDG in PC-3 with or without phlorizin inhibition, after being grown for three days in either low (2.5mM), medium (11.5mM), or high (25mM) glucose. Results show noticeably lower uptake in high glucose, suggesting that SGLT is more active when grown in low glucose conditions

With the evidence that SGLT activity might be connected to survival mechanisms for these cancer cell lines, we started growing the cells under various stressful conditions, to look for either effects on SGLT activity or for conditions during which SGLT activity is either helpful or detrimental to survival. Attempts at starving cells both of glucose and media serum showed inconclusive results, with SGLT activity increasing in starved conditions, but highly variable.

	high gluc	low gluc	high gluc serum starved	low gluc serum starved
□ Control	88.8	99.2	83.9	195.8
■ Phlorizin	59.3	72.0	62.0	131.1
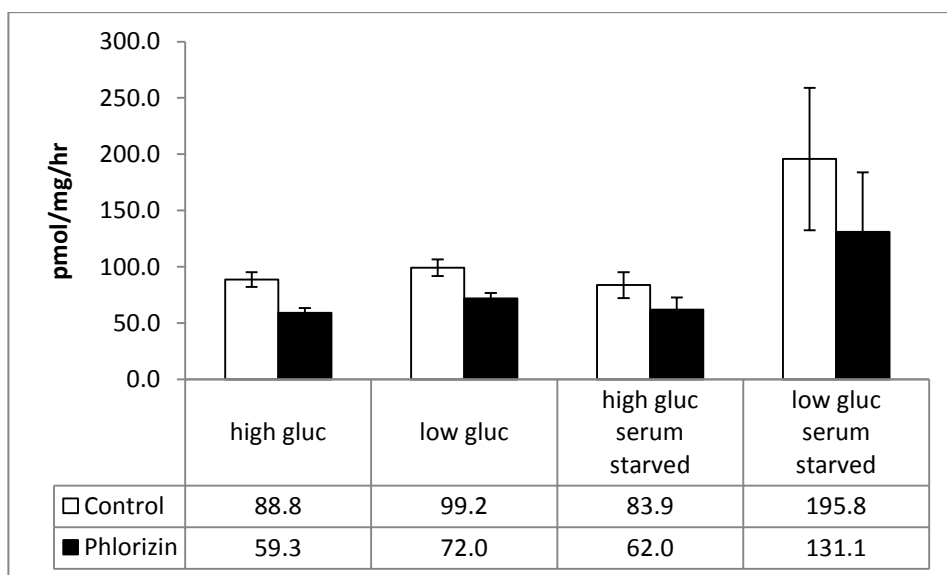
Figure 23: SGLT activity of PC-3 with either glucose or serum starvation. Results show some increase of SGLT during starved conditions, but results are highly variable.

3.5.2 Cell survival assay suggests SGLT does not affect survival in simulated hypoxic conditions

Since hypoxia is a common condition in cancer tumors that has a significant impact on metabolic requirements, we decided to test the usefulness of SGLT activity under simulated hypoxic conditions. To simulate hypoxia, cells were grown in the presence of cobalt chloride, which simulates hypoxic conditions in culture. Cells were grown with or without cobalt chloride, and with or without phlorizin, in 2.5mM glucose, to determine if SGLT activity is useful or

detrimental to cell survival. As shown in Figure 24, phlorizin did not show a statistically significant

effect on cell death or growth rates with or without cobalt chloride after 2 days.

Percent cell death after 2 days

	Control	Cobalt Chloride
□ Control	1.84%	5.78%
■ Phlorizin	2.27%	6.84%
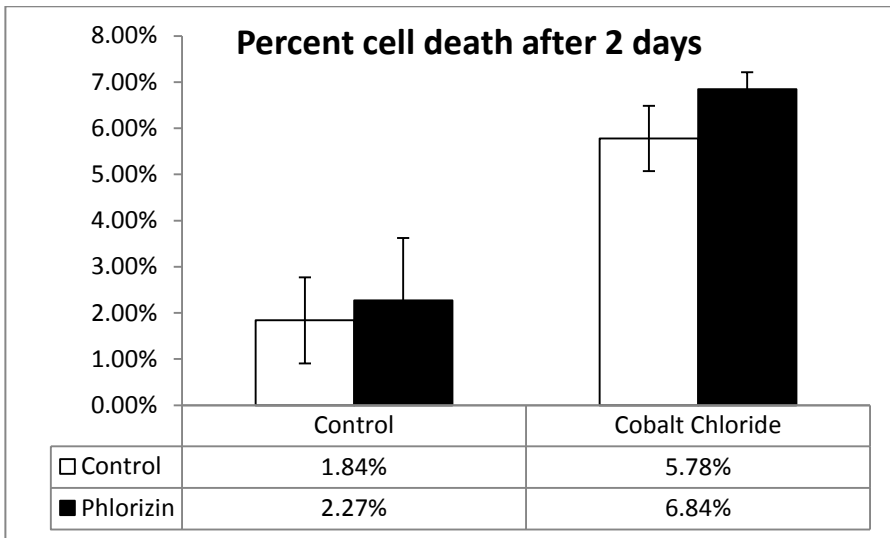
Figure 24: Cell survival assay in pancreatic cancer cell line using cobalt chloride to simulate hypoxic conditions. Results show SGLT plays little role in surviving hypoxic conditions.

3.6 Regulatory Protein Connections

Identifying regulatory connections to SGLT activity has the potential to be very useful for providing insight into treatment options, so we wanted to test for changes in SGLT activity in response to regulatory protein activation or inactivation.

3.6.1 SGLT activity shows no response to PKA or PKC activation

The first connection we tested for was any influence PKA or PKC had on SGLT activity in either PC-3 or AsPC-1 cell lines. PKA and PKC are both activators of SGLT1 and SGLT2 activity in humans[81,82], so we tested the effects of PKA activator 8-Bromoadenosine 3',5'-cyclic monophosphate (8-Br-cAMP) and PKC activator sn-1,2-dioctanoylglycerol (DOG) on phlorizin dependent uptake *in vitro*. Cells were incubated for one hour with either 1μM DOG or 100μM 8-Br-cAMP, then tested for αMDG uptake. As shown in Figure 25, there was no change in SGLT activity in response to either activator, indicating SGLT activity independent of either PKA or PKC.

	PC-3 control	PC-3 + DOG	PC-3 + 8BrrCAMP	AsPC-1 control	AsPC-1 + DOG	AsPC-1 + 8BrrCAMP
☐ Control	166.5	134.0	140.3	171.5	177.4	170.1
■ +phlorizin	120.8	91.4	96.1	104.9	97.3	123.9
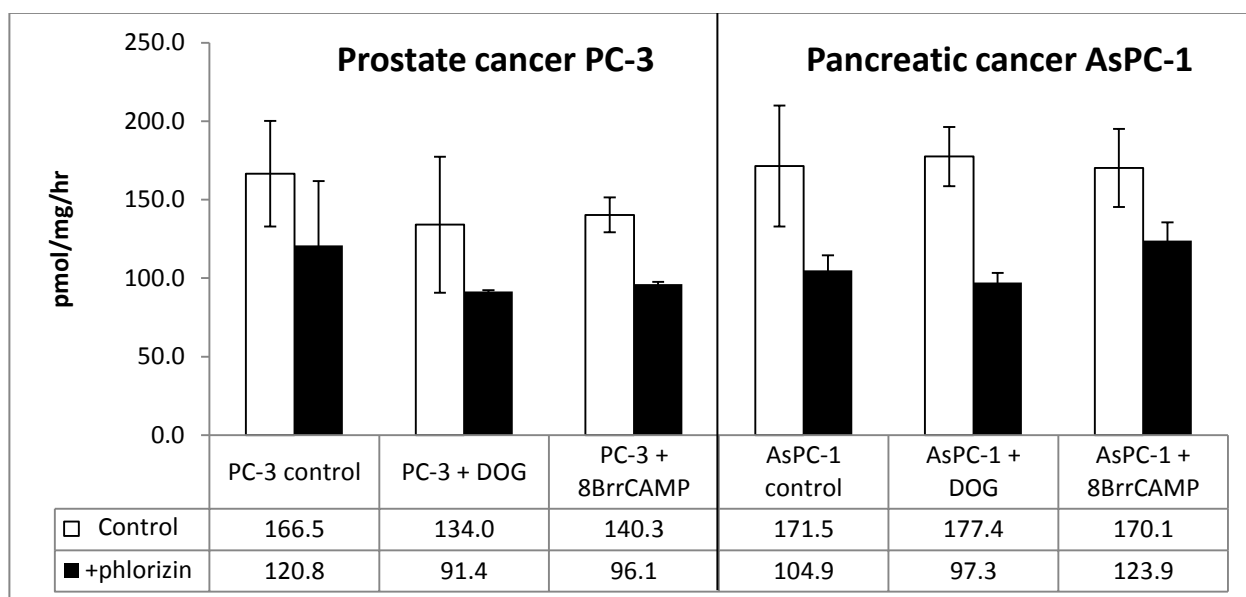
Figure 25: Phlorizin dependent αMDG uptake in AsPC-1 and PC-3 cells in the presence of PKA or PKC activators. Results show no increased SGLT activity with activation of PKA or PKC, confirming previous results of lack of SGLT1 or SGLT2 dependent uptake.

3.6.2 EGFR inhibition by erlotinib has inconsistent effect on SGLT activity

Since EGFR has also been implicated in SGLT function in cancer, we the EGFR kinase inhibitor erlotinib on SGLT activity. Cells were grown with either 0, 10, or 20μM erlotinib for 1 day, and then tested for αMDG uptake. As shown in Figure 26, initial tests suggest erlotinib has a slight effect on SGLT activity, with lower SGLT activity observed at higher erlotinib concentrations. However, further tests showed inconsistent effects *in vitro* upon repeated experiments, with some tests showing no significant decrease in αMDG uptake with EGFR inhibition.
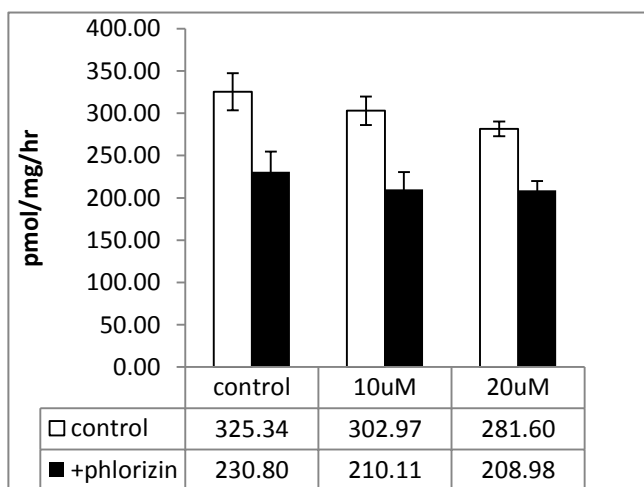
	control	10uM	20uM
□ control	325.34	302.97	281.60
■ +phlorizin	230.80	210.11	208.98

Figure 26: Phlorizin dependent αMDG uptake in AsPC-1 cells grown with either 0uM, 10uM, or 20uM EGFR inhibitor erlotinib. Results show slight inhibition of SGLT function.

The results of the regulatory protein tests showed poor response in cell culture tests. Due to these results, as well as the vast difference between cell culture and *in vivo* behavior in models, further tests on regulatory protein connections were abandoned. While these initial cell line tests were useful for identifying cell lines to use in animal models, they also make it clear that *in vivo* experiments are essential for determining the activity of SGLTs in cancer tumors reliably.

3.7 Xenografts

With success from the *in vitro* experiments in identifying cell lines demonstrating SGLT activity, we next began tests in animal models. Mice were injected with either AsPC-1 or PC-3 xenografts, and scanned with Me-4FDG or 2-FDG PET, as well as CT after tumors developed.

3.7.1 Pancreatic and Prostate xenografts display Me-4FDG uptake

Seven mice with tumors from each cell line, AsPC-1 and PC-3, were used in testing for SGLT activity in xenografts, denoted AsPC1-7 and PC1-7. Results of fused Me-4FDG PET/CT dynamic scans showed significant uptake of Me-4FDG in all fourteen xenografts, allowing clear imaging of the tumors in each mouse. Figure 27 shows three examples of each, AsPC2, 3, and 5 for pancreatic cancer, and PC1, 2, and 3 for prostate cancer (threshold range 1.3-1.7 SUV to distinguish tumors from surrounding signal). SUV was calculated for regions drawn around each of the tumors over time, with tumors showing consistent SUV increase over the course of the entire one hour dynamic scan. Final SUVs by the
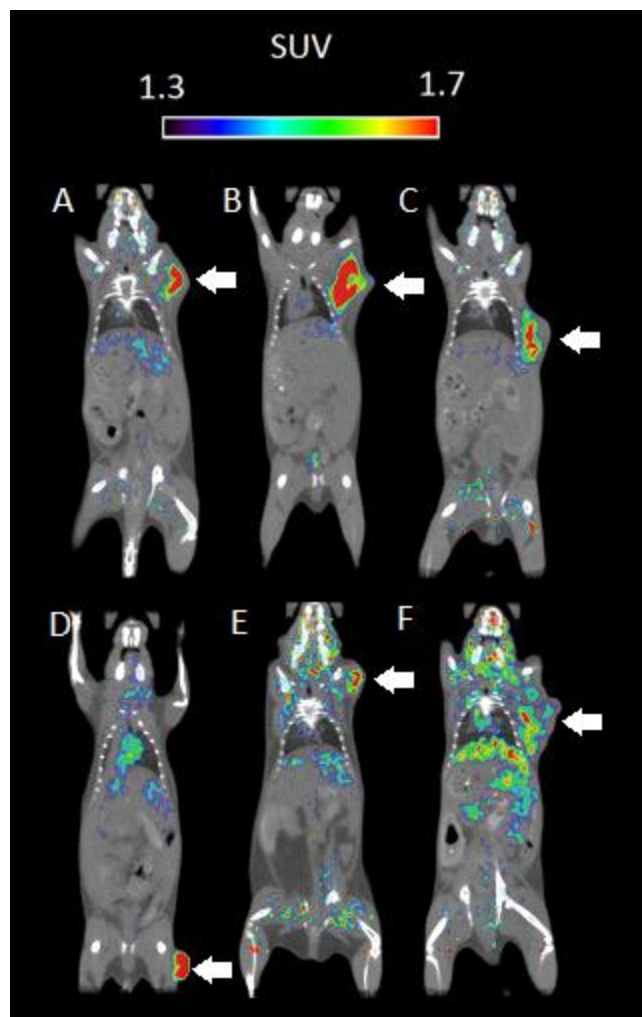
Figure 27: Me-4FDG PET scans 1 hour after injection for mice (A) AsPC2 (B) AsPC3 (C) AsPC5 (D) PC1 (E) PC2 (F) PC3. Each scan shows significant uptake of Me-4FDG in tumor regions compared with other organs, suggestion functional expression of SGLTs.

end of the dynamic scan varied widely, but averaged between 1.2 and 1.4, with portions of some tumors reaching above 1.7, well above the background signal in muscles and other organs. This constant increase confirms expression of active SGLTs.

3.7.2 Xenograft tumors have higher Me-4FDG SUV than 2-FDG

Once we established the presence of functional SGLTs in xenografts, we next wanted to compare the strength of Me-4FDG imaging to conventional 2-FDG imaging. Figure 28 shows average SUV (decay corrected) over time for all Me-4FDG and 2-FDG PET scans, normalized to total injected signal. All of the AsPC-1 xenografts showed much stronger Me-4FDG uptake than 2-FDG, with 2-FDG uptake peaking after 10-15 minutes, and then decreasing. In contrast, average SUVs from PC-3 xenografts demonstrated no significant difference between Me-4FDG and 2-FDG.
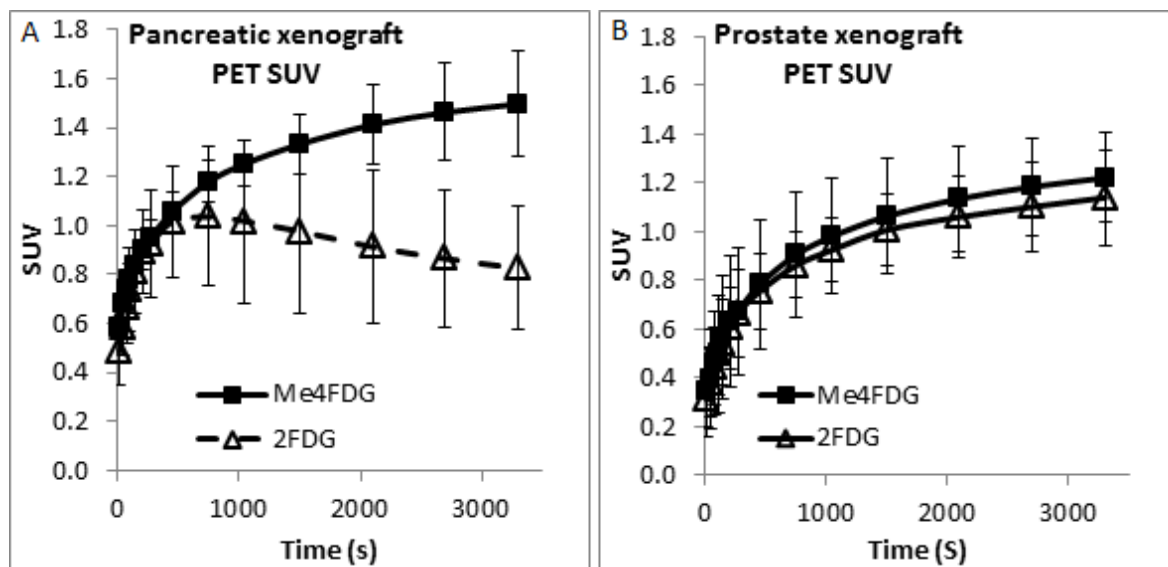
Figure 28: Decay corrected Me-4FDG vs 2-FDG signal in pancreatic and prostate xenografts over 1 hour period after injection. (A) Average Me-4FDG and 2-FDG signal in AsPC mice. Signals show significantly higher Me-4FDG accumulation in pancreatic tumors than 2-FDG. (B) Average Me-4FDG and 2-FDG signal in PC mice. Signals show no statistically significant difference. Standard deviation used for error bars.

Since the 2-FDG profile of the PC-3 xenografts was markedly different than that of the AsPC-1 xenografts, we wanted to confirm that the difference was not due to any change in
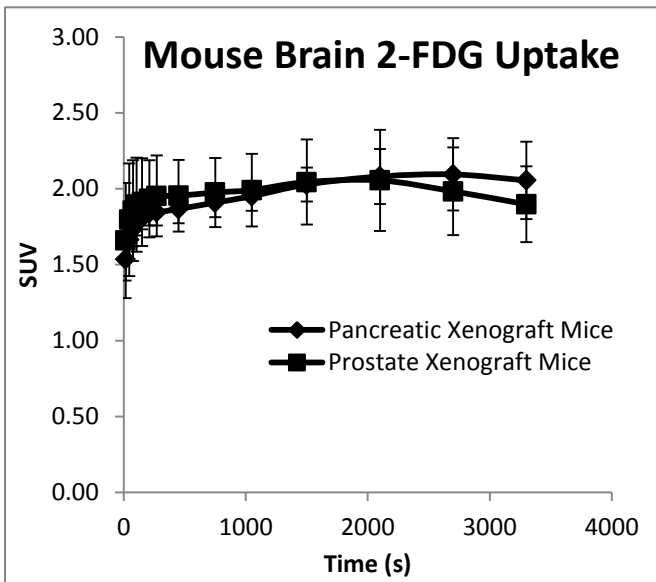
Figure 29: Decay corrected 2-FDG uptake in mice brains shows no significant difference in bioavailability of 2-FDG in mice with pancreatic verses prostate tumors, indicating difference in 2-FDG SUV in tumors is not due to bioavailability of 2-FDG

bioavailability of 2-FDG, but specifically due to the difference in tumor biology. 2-FDG is strongly taken up in the brain, making the brain an ideal organ to use to compare bioavailability from one mouse to the next. Figure 29 shows brain SUV for 2-FDG scans for mice with either pancreatic tumors or prostate tumors, showing no significant difference in 2-FDG uptake in the brain. Comparing other organs such as heart or liver yields the same results, with no significant variation from one animal to the next. With no difference in bioavailability of 2-FDG from mouse to mouse, it's clear that the difference in tumor uptake of 2-FDG is due solely to differences in tumor biology, and not differences between individual mice.

3.7.3 Prostate cancer tumors demonstrate variation in SUV for 2-FDG or Me-4FDG

The contrast between pancreatic and prostate xenografts in comparing GLUT vs SGLT activity presented an interesting problem. Since there was variation from tumor to tumor, we next tested whether or not Me-4FDG and 2-FDG SUV variation was random or related. One of our initial theories at the start of this project was that SGLT activity might compensate for a lack of GLUT activity, so we wanted to compare the activity of each tumor with each imaging probe to see if we saw that predicted trend. Figure 30 shows activity curves for 4 mice of each cell line that we have both 2-FDG and Me-4FDG scans of. Interestingly, in the pancreatic cancer xenografts,
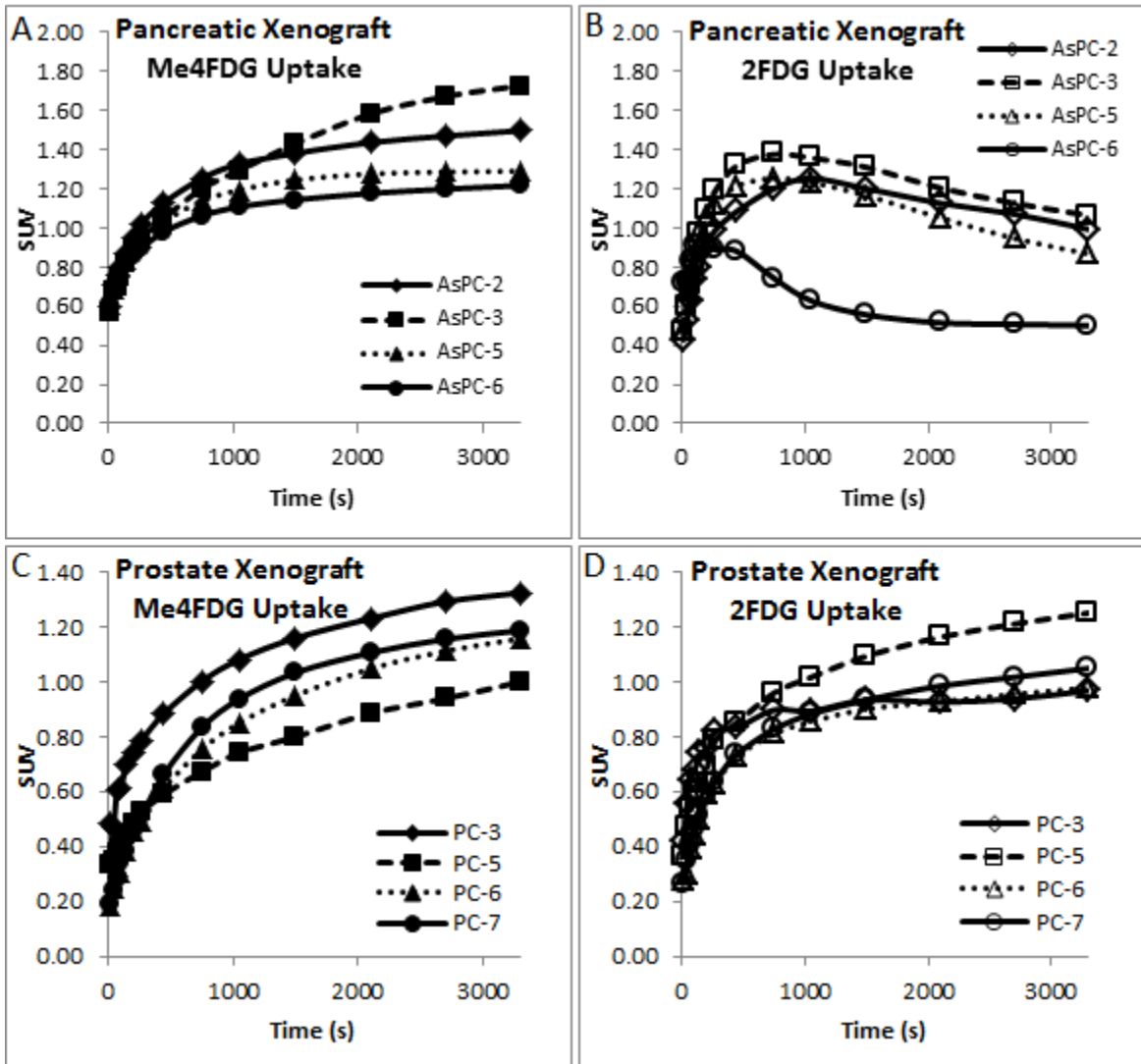
Figure 30: Decay corrected Me-4FDG uptake in pancreatic and prostate cancer xenografts compared with 2-FDG uptake over the course of 1hr PET scan. (A) Me-4FDG SUV shows consistent SGLT activity among pancreatic cancer xenografts. (B) 2-FDG SUV shows low 2-FDG retention in pancreatic cancer xenografts. Noticeably, the mouse with the lowest Me-4FDG signal pancreatic xenograft also has the lowest 2-FDG signal, while the mouse with the highest Me-4FDG signal also has the highest 2-FDG signal. (C) Me-4FDG SUV shows all prostate cancer xenografts demonstrating significant Me-4FDG uptake. (D) Prostate cancer xenografts show lower 2-FDG SUV than Me-4FDG SUV, with the exception of PC5 demonstrating higher than average 2-FDG SUV, with lower than average Me-4FDG SUV.

the mouse with the highest Me-4FDG uptake (AsPC3) also had the highest 2-FDG uptake, while

the mouse with the lowest Me-4FDG uptake (AsPC6) also had the lowest 2-FDG uptake. This

trend was strikingly reversed in the prostate cancer animal model, with the tumor from PC5

showing relatively higher 2-FDG SUV and the lowest Me-4FDG uptake. These trends hold true

even when normalized to SUV of the brain or muscles, showing that this is due to tumor biology, and not simply availability of the particular imaging probe. Although PC5 remains an outlier relative to the other prostate cancer mice, this deviation hints at an intriguing possibility that, in some cases, relative preference for GLUT or SGLT uptake of glucose may be a product of tumor development, and not merely the genetic profile of the initial cells. In the AsPC-1 xenografts, it seems that both GLUT and SGLT activity are both linked to overall tumor metabolic rate, and not necessarily inversely correlated. In either event, we have examples here of tumors for both prostate and pancreatic cancer that are demonstrating functional use of sodium glucose transporters. Figure 31 shows coronal and transverse cross-sections of Me-4FDG and 2-FDG PET scans of AsPC3 and AsPC6, the mice with the highest and lowest tumor activity respectively, at 15 minutes and 60 minutes post injection. The 2-FDG signal peaks at about 15 minutes post injection, while Me-4FDG continues to accumulate.

Figure 32 shows coronal and transverse cross-sections of Me-4FDG and 2-FDG PET scans for PC3 and PC5. The scans confirm the results of the uptake curves, with PC3 showing a higher SUV for Me-4FDG than PC5, and PC5 showing a higher SUV for 2-FDG than PC3. Also of note, different regions of the tumors show different SUVs for active or passive glucose transport, supporting the theory that SGLT activity might be used as an alternative to GLUT uptake in certain conditions. Even after comparing tumor SUV to organ SUV for each mice, these differences between specificity in tumors remains distinct. Thus we have clear examples of pancreatic cancer tumors generated from both AsPC-1 and PC-3 cell lines displaying use of SGLT for glucose uptake to an extent significant enough to image using PET.
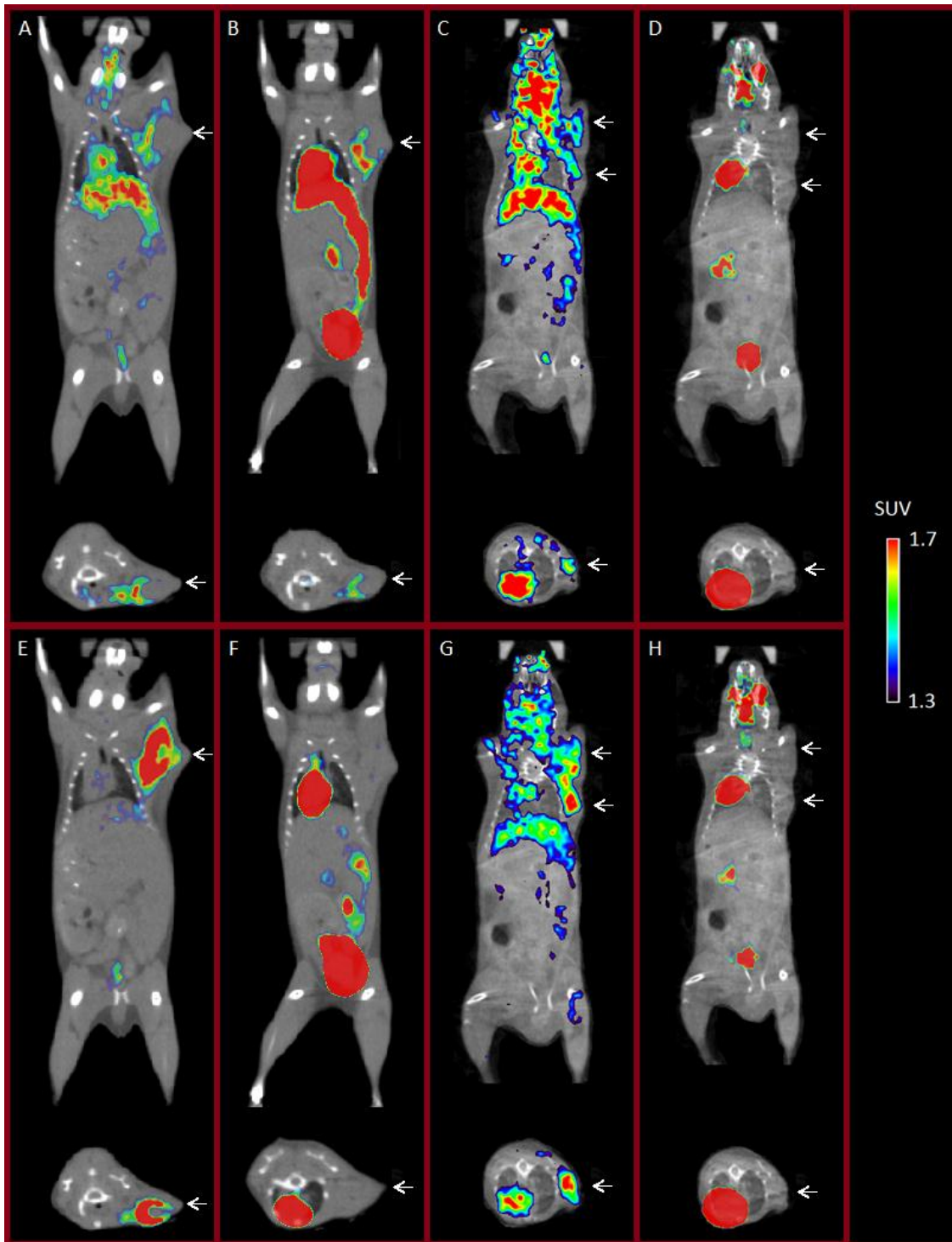
Figure 31: PET scans of mice with pancreatic cancer tumors. Tumors indicated by white arrows. Scan of mouse AsPC3 with Me-4FDG at (A) 15 min and (E) 60 min and 2-FDG at (B) 15 min and (F) 60 min and mouse AsPC6 with Me-4FDG at (C) 15 min and (G) 60 min and 2-FDG at (D) 15 min and (H) 60 min. In all mice with pancreatic cancer, Me-4FDG uptake was stronger than 2-FDG uptake. AsPC3 tumor had highest Me-4FDG and 2-FDG uptake, while AsPC6 had the lowest uptake for both Me-4FDG and 2-FDG.
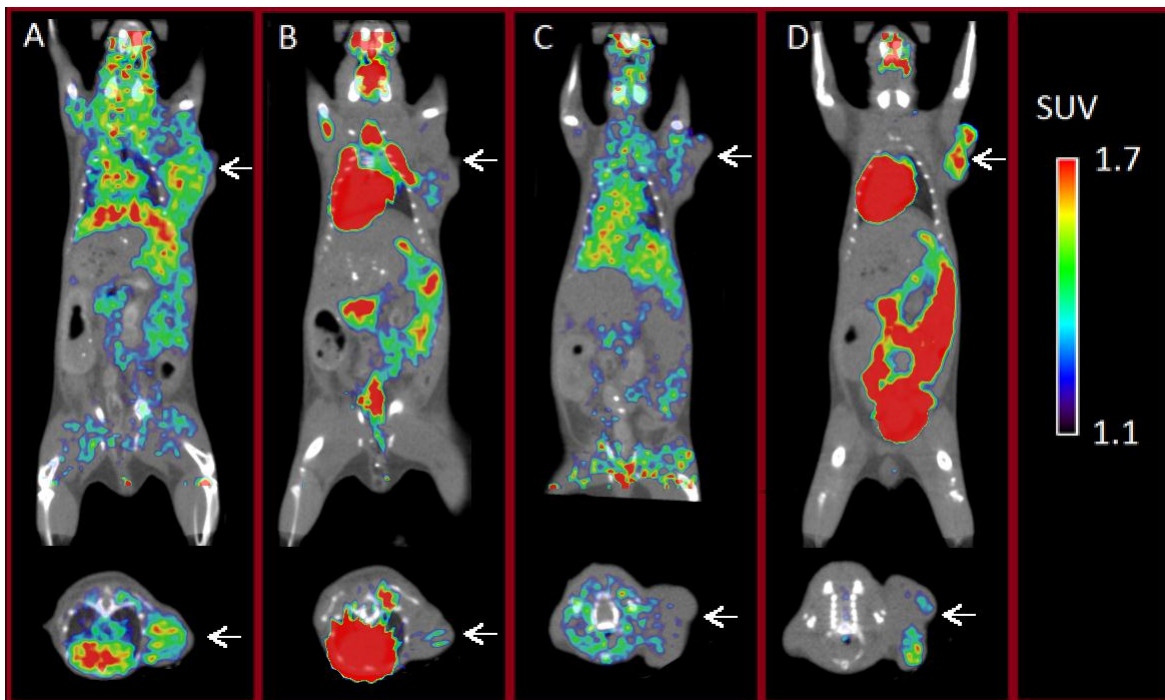
Figure 32: PET scans of mice with prostate cancer tumors one hour after PET injection. Tumors indicated by white arrows. Scan of mouse PC3 with (A) Me-4FDG (B) 2-FDG and mouse PC5 with (C) Me-4FDG (D) 2-FDG. PC3 had the highest Me-4FDG uptake and average 2-FDG uptake, while PC5 had above average 2-FDG uptake and the lowest Me-4FDG uptake. This suggests that the level of SGLT or GLUT uptake of glucose develops after initial development of disease, since these tumors were each started from the same cell line under identical conditions.

3.7.4 Autoradiography and immunohistochemistry correlate with tumor heterogeneity

Identifying tumors with different transporter activities raises the question of whether or not these tumors express GLUT or SGLT proteins correlating with this variation, or if some other aspect of cell metabolism dictates heterogeneity of 2-FDG or Me-4FDG accumulation. Figure 34 shows PET analysis of tumors from PC7, which showed average Me-4FDG and 2-FDG uptake, compared with GLUT1 and GLUT3 protein staining in 7uM tumor slices. GLUT staining in slices containing the full length of the tumor showed fairly even distribution, with some spots showing slightly stronger staining. Compared with 2-FDG PET, this is fairly consistent with the presence of GLUT activity. Noticeably, lowering the minimal threshold for Me-4FDG and 2-FDG signal in the PET scans shows regions with higher or lower relative preference for one probe or the other.

Likewise, there is some noticeable variation in GLUT expression in tumor slices. While these results cannot be used to directly compare GLUT expression and activity to SGLT expression and activity, since PET and immunohistochemistry don't provide information that can quantifiably compare activity and expression between different proteins, we can use PET images and protein staining to compare different tumor regions relative to each other, and identify correlations between *in vivo* transporter activity and transporter expression. These show quite clearly that there is variation in glucose transport in tumors not just between different mice and different cancers, but also within different regions in the same tumor. No definitive inverse correlation between Me-4FDG and 2-FDG SUV in scans can be seen, indicating that SGLT activity likely plays some role in tumor biology beyond simply offsetting a lack of GLUT activity.
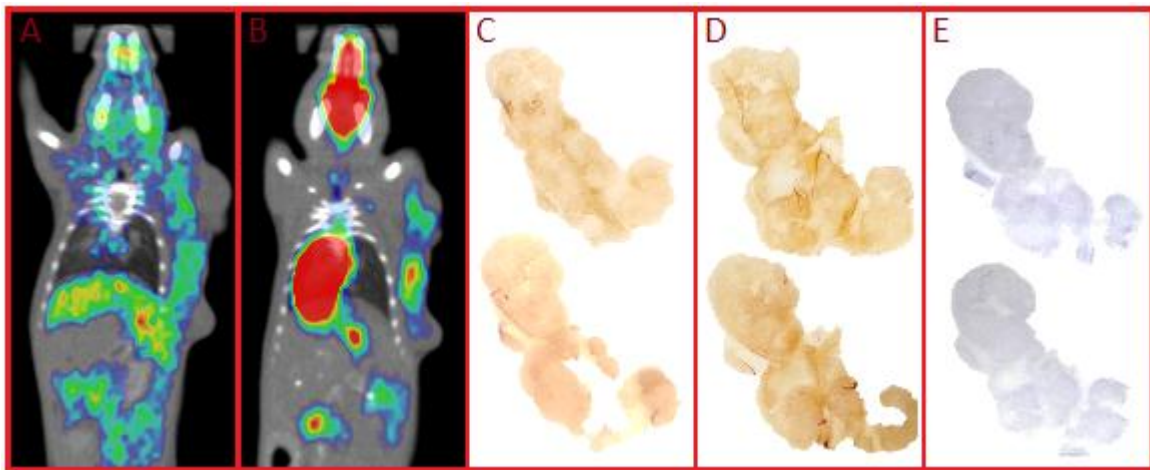
Figure 33: Me-4FDG and 2-FDG PET scans with GLUT staining for PC7. (A) Me-4FDG PET scan, scale 1.1-1.6 SUV (B) 2-FDG PET scan, scale 0.9-1.7 SUV. (C) GLUT1 shows strong signal evenly distributed throughout tumor. (D) GLUT3 staining shows fairly even distribution, with some pockets of stronger expression. (E) Negative control. Results show expression of both GLUT1 and GLUT3 across tumor, but also identify regions with preferential uptake of either 2-FDG or Me-4FDG.

With PET scans showing signs of variation in transporter activity in different tumor regions, we continued to test for evidence of tumor heterogeneity by comparing Me-4FDG uptake more precisely in tumor slices to glucose transporter protein expression, using *in vivo* Me-4FDG

uptake. Thirty minutes after additional 1 mCi Me-4FDG injection, animals were sacrificed and tumors excised, frozen, and sliced. Figure 34 shows autoradiography for tumor slices from PC3, the prostate cancer xenograft with

Figure 34: Autoradiography of Me-4FDG accumulation in tumor *in vivo* for slices of PC3 tumor. Results show selective uptake of Me-4FDG in certain tumor regions.

the highest observed Me-4FDG SUV, clearly identifying different regions of the tumor with higher relative uptake of Me-4FDG. GLUT1 and GLUT3 staining from a different section of the same tumor (data not shown) also shows selective regions of GLUT1 expression, with GLUT3 being more evenly distributed throughout the tumor. While cell morphology is poorly preserved through the autoradiography process, these regions can still be identified as distinct, and demonstrate the presence of different regions that preferentially either display SGLT activity or GLUT1 expression. Additional tests on other tumor xenografts yield similar results. Figure 35 shows GLUT staining for AsPC6, which displayed both weak Me-4FDG and 2-FDG uptake in PET scans. In this case, GLUT staining shows less variation from one tumor region to the next.

The presence of different tumor regions and activity was highly pronounced in PC6. Figure 36 shows PET scans, autoradiography, and GLUT1 and 3 staining for PC6, with PET signal thresholds scaled down to highlight the regions of the tumor with variation in SUVs. Again, regions with higher SUV 2-FDG had lower SUV for Me-4FDG, and vice versa. GLUT1 signal had stronger variation than GLUT3, suggesting that GLUT1 might have a higher impact on 2-FDG accumulation than GLUT3. In particular, the region of the tumor that showed the least Me-4FDG uptake in the tumor slices used for autoradiography seemed to also have higher GLUT1 expression, correlating with the trend observed in PET scans.
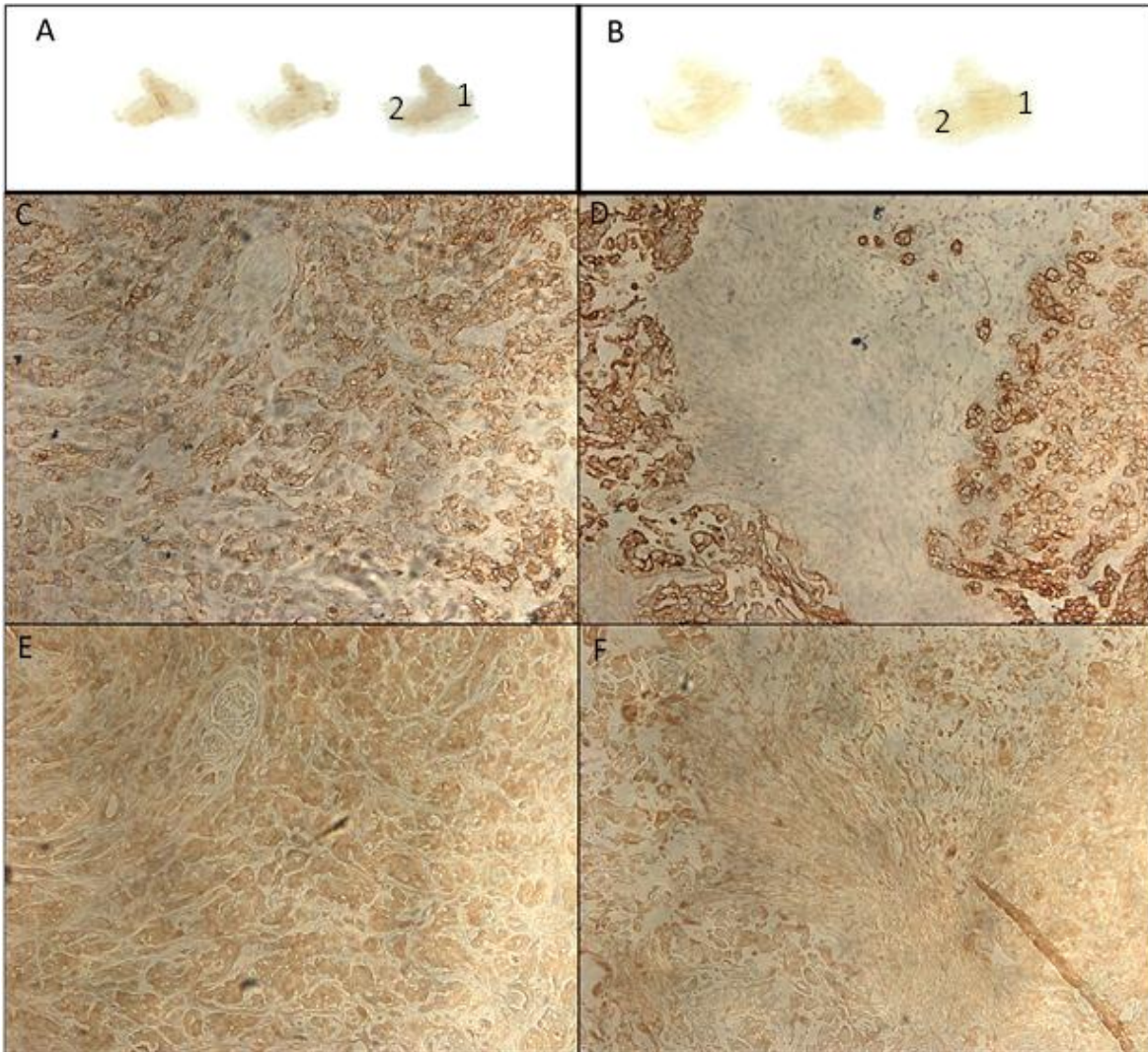
Figure 35: GLUT protein staining for slices of AsPC6 tumor. (A) GLUT1 staining in tumor slices. (B) GLUT3 staining shows weaker signal than GLUT1. (C) Magnification of region 1 with GLUT1 staining. (D) Magnification of region 2 with GLUT1 staining. (E) Magnification of region 1 with GLUT3 staining. (F) Magnification of region 2 with GLUT3 staining.

While the process of freezing and slicing the tumor prevented effective preservation of tumor morphology in each of the xenograft tumor samples throughout all mice, the combination of PET scans, autoradiography, and protein staining shows consistently that there are different tumor regions that can be identified with both 2-FDG and Me-4FDG uptake and immunohistochemistry staining. These results mark the first time the presence of tumor regions

with altered activity of passive and active transporters of glucose have been identified, and open

a novel avenue for future exploration of tumor heterogeneity.
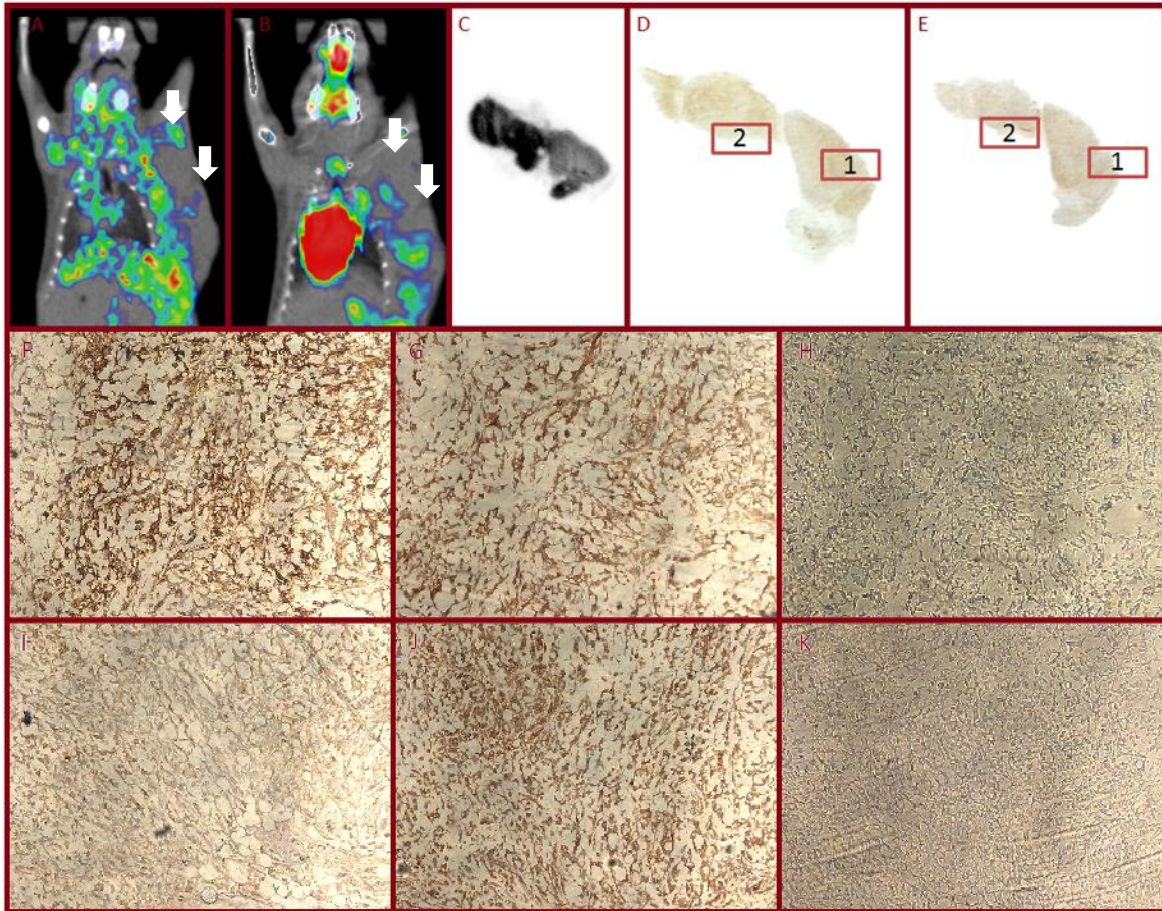
Figure 36: PET scans, autoradiography, and GLUT staining from PC6. (A) Me-4FDG PET scan, scale 1.2-1.6 SUV (B) 2-FDG PET scan, scale 0.9-1.5 SUV (C) Autoradiography of Me-4FDG accumulation *in vivo* (D) GLUT1 staining on 7uM tumor slices (E) GLUT3 staining on 7uM slices (F) Magnification of GLUT1 staining in region 1 (G) Magnification of GLUT3 staining in region 1 (H) Magnification of negative control in region 1 (I) Magnification of GLUT1 staining in region 2 (J) Magnification of GLUT3 staining in region 2 (H) Magnification of negative control in region 2. GLUT1 demonstrates higher variation in staining in different regions, suggesting it may play a greater role in tumor heterogeneity.

3.7.5 SGLT2 inhibition by dapa reduces tumor uptake of Me-4FDG, but also reduces bioavailability of Me-4FDG

While initial *in vitro* tests with cell lines were unable to identify the active SGLT responsible for Me-4FDG uptake, initial immunohistochemistry staining in tumor slices showed SGLT2 to be highly expressed in several tumor regions. With the observation of SGLT2 staining, we decided to try testing for SGLT2 activity *in vivo* by injecting animals with dapa before, after, or with Me-4FDG injection, to test for inhibition of Me-4FDG accumulation in xenografts. As shown in Figure 37, the presence of dapa drastically reduced tissue retention of Me-4FDG in xenografts, further implicating SGLT2 as a contributor to Me-4FDG accumulation in tumors.
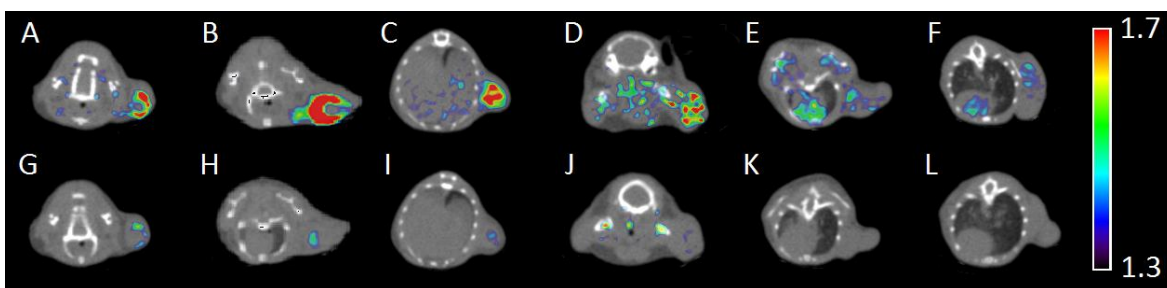
Figure 37: PET scans of Me-4FDG with or without dapa inhibition of SGLT2. Without inhibition: (A) AsPC2 (B) AsPC3 (C) AsPC5 (D) PC2 (E) PC6 (F) PC7. With inhibition: (G) AsPC2 (H) AsPC3 (I) AsPC5 (J) PC2 (K) PC6 (L) PC7. Scans show significant loss of Me-4FDG uptake after dapa injection.

Time-activity curves shown in Figure 38 demonstrate the significantly reduced uptake in Me-4FDG in animals injected with 1 mg/kg dapa in both pancreatic and prostate cancer xenografts. However, since dapa should also inhibit Me-4FDG recycling in the kidneys through SGLT2, we needed to confirm that the drop in Me-4FDG uptake was specifically due to inhibition of SGLT2 in the tumors, and not simply a drop in bioavailability of Me-4FDG. Analysis of signal accumulation in the bladder, shown in Figure 39, confirms that 33% (+/- 5%) of Me-4FDG accumulated in the bladder over the course of the scan when SGLT2 was inhibited by dapa, as opposed to only 2% (+/-1%) without dapa inhibition.
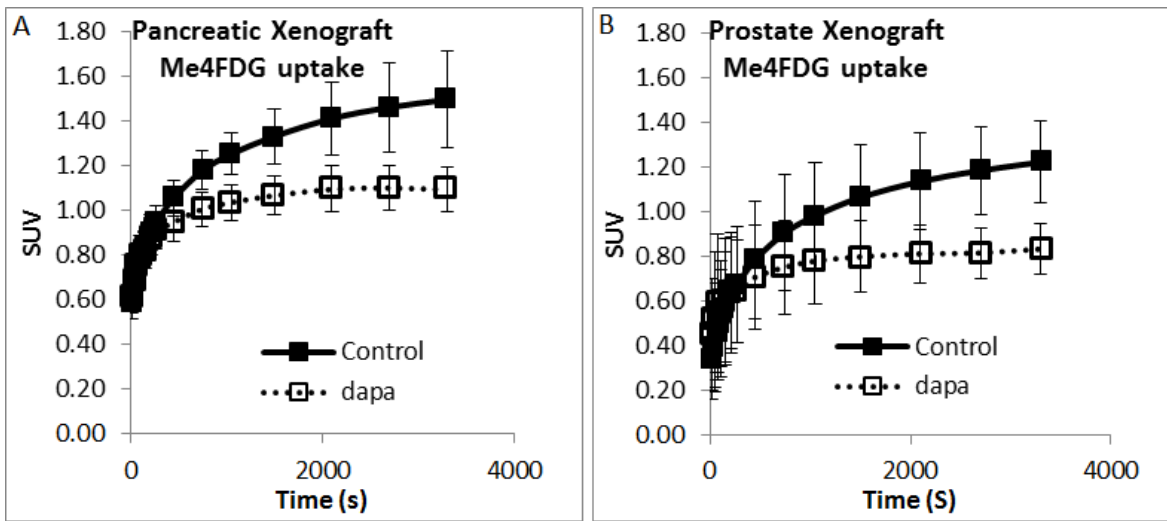
Figure 38: Average Me-4FDG accumulation time-activity curve with or without dapa inhibition in either (A) Pancreatic cancer xenografts or (B) Prostate cancer xenografts. Results show noticeable inhibition of Me-4FDG uptake by dapa.

With this drastic reduction in bioavailability of Me-4FDG observed in these scans, we compared changes in tumor Me-4FDG accumulation to that of other organs in the presence of dapa, to see if there was a noticeably higher decrease in tumors than in other organs. Figure 40 shows average Me-4FDG accumulation in mouse brains and leg muscles (averages of front left leg and right rear leg). No significant difference was observed in Me-4FDG accumulation between front and rear legs, so results were averaged for each mouse. There is a noticeable decrease in Me-4FDG accumulation in
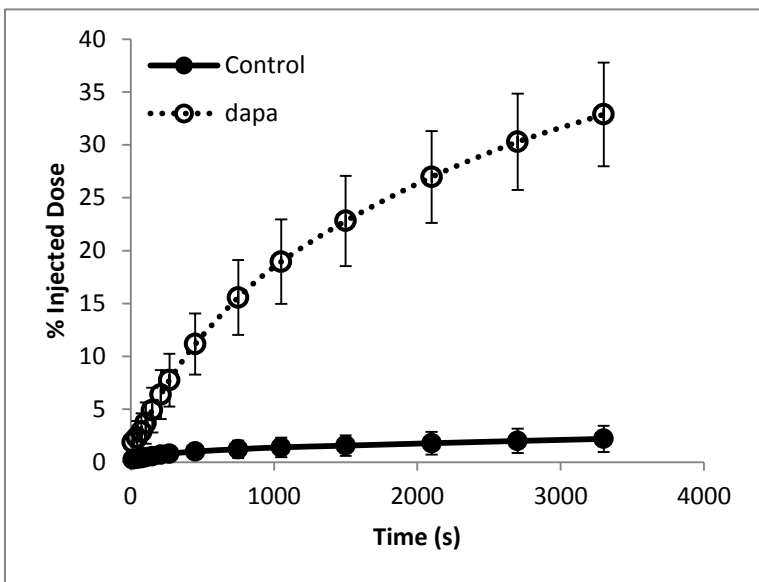
Figure 39: Percent injected dose of Me-4FDG accumulation in the bladder for mice with or without 1 mg/kg dapa inhibition. Results show inhibition of SGLT2 in kidneys results in a loss of roughly 30% on the injected Me-4FDG over the course of the scan.

61

response to dapa (even in the brain where no Me-4FDG accumulates), showing that there is some drop in signal resulting from the loss of Me-4FDG to the bladder. The fact that Me-4FDG does accumulate in muscles shows that there is some SGLT activity present in muscle as well as tumors, and dapa alone at 1mg/kg concentration is not sufficient to completely eliminate SGLT activity present.
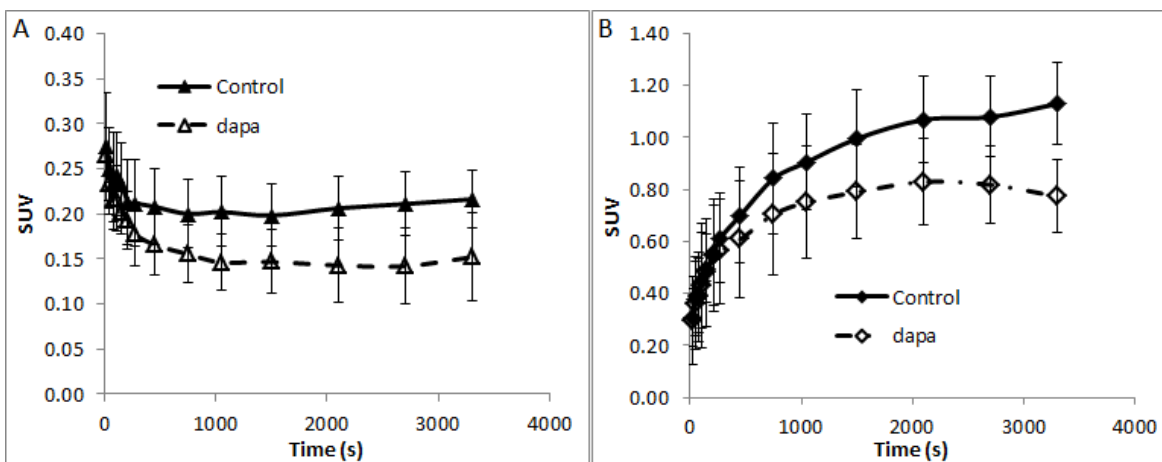
Figure 40: Average Me-4FDG SUV in (A) brain and (B) leg muscles with or without dapa inhibition. Results show wide variation from mouse to mouse, but noticeable decrease in SUV with dapa injection in both brain and muscles. The decrease in brain and muscle isn't quite as pronounced as in tumors with high Me-4FDG uptake, suggesting that there is some inhibition of tumor uptake in response to dapa beyond simply decrease in bioavailability.

Since there was noticeable drop in Me-4FDG uptake in each organ and tissue in response to the drop in bioavailability, we wanted to confirm that the drop in tumor uptake was due at least partly to dapa inhibition, and not loss in bioavailability. In order to test this, we compared SUV data from scans that used different concentrations of dapa used to inhibit SGLT2. Rather than using 1mg/kg dapa to inhibit, mice PC6 and PC7 were injected with 0.5mg/kg dapa and 0.2mg/kg dapa respectively, which would reduce the amount of Me-4FDG built up in the bladder, as shown in Figure 41. With lower buildup in the bladder, and thus higher bioavailability, we then

compared muscle and tumor dapa sensitivity for PC7, to see if tumors showed greater sensitivity to inhibition than muscle tissue.

Averaging three different sections of the tumor in PC7 revealed a noticeable drop in tumor SUV in response to dapa. In contrast, there was no noticeable drop in muscle SUV from either front left or right hind leg, shown in Figure 42. As expected, the 0.5 mg/kg dapa
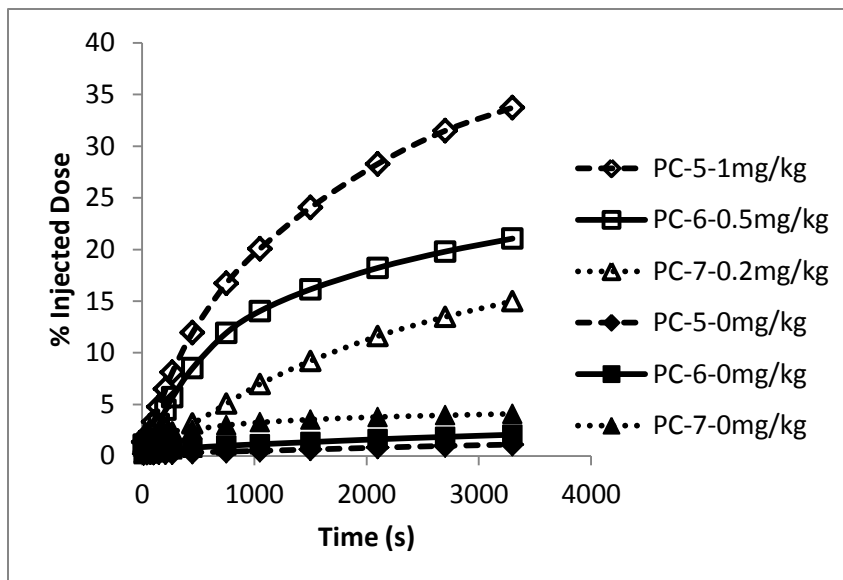
Figure 41: Percent injected dose of Me-4FDG accumulation in the bladder for mice with or without dapa inhibition at different concentrations. Results show decreasing concentration of dapa significantly reduces buildup of Me-4FDG in bladder.

inhibited PC6 scan showed slightly lower SUV than 0.2 mg/kg dapa inhibited PC7, and slightly higher SUV than other dapa inhibited scans, consistent with the conclusion that bioavailability plays a role in tissue signal, and is sensitive to dapa levels. Taken together, these results demonstrate at least some level of sensitivity to dapa in tumors independent of bioavailability, implicating SGLT2 as a contributing factor in tumor Me-4FDG uptake. While the drop in Me-4FDG SUV in response to dapa in each organ and tissue is clearly partly due to lower bioavailability of Me-4FDG, there is a noticeable contribution by SGLT2 specifically in tumor SGLT activity that seems to be more observable at lower concentrations of dapa.

Combined with the protein staining of SGLT1 and 2, the Me-4FDG PET scans with or without dapa implicate SGLT2 as having at least a partial role in tumor SGLT activity. While it is possible that there are other unidentified SGLTs active in these tumors, since dapa alone is not sufficient to completely halt all Me-4FDG uptake, it is also possible higher dapa concentration is required to completely inhibit SGLT2 activity.
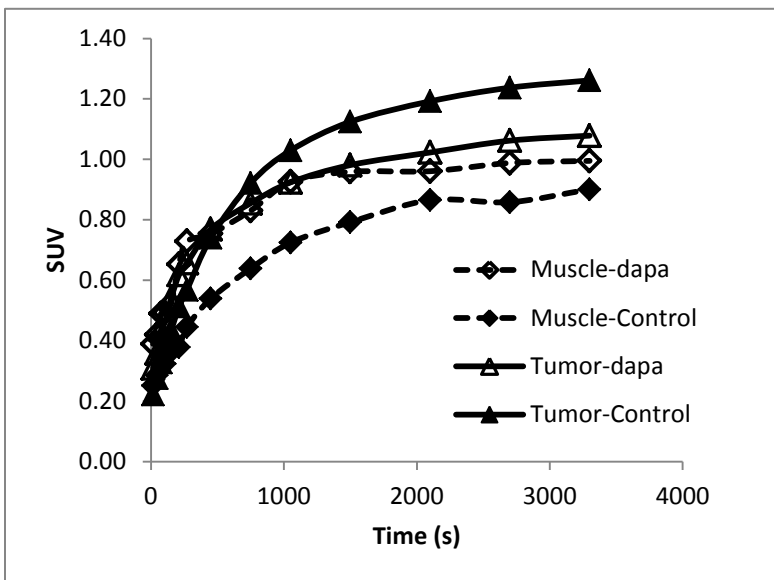
Figure 42: Me-4FDG SUV in tumor and muscle from PC7 with or without 0.2mg/kg dapa. Results show a significant decrease in tumor SUV in response to dapa, but no decrease in muscle SUV, indicating that tumors have a higher sensitivity to dapa than muscle.

3.8 Conclusions

These results mark the first evidence confirming SGLT activity in cancer *in vivo*, and the first evidence identifying dapa sensitive SGLT activity in cancer. Not only have we confirmed that sodium glucose transporters are active in these prostate and pancreatic xenografts, we have also found evidence that SGLT activity is higher in certain tumor regions than others. In complementary work conducted by Dr. Claudio Scafoglio on this project, SGLT2 protein was found to also be expressed in these xenografts with high Me-4FDG uptake, in regions roughly matching the Me-4FDG retention observed in the autoradiography tests. While these regions didn't always relate inversely to GLUT protein staining, we now have evidence that at least in some tumors SGLT and GLUT proteins are overexpressed in different regions of tumors and are likely responsible for the variability in Me-4FDG and 2-FDG uptake in PET scans. This raises a very interesting question as to why tumors might prefer utilizing SGLTs in these particular regions as opposed to others. SGLTs use energy to transport glucose, and would seem to be inefficient to use when GLUT transporters are available.

Unfortunately, we were unable to confirm one of our theories that Me-4FDG will be expressed more highly in regions with low glucose concentrations, as the conditions of the tumors after excision did not allow for measuring glucose levels in different tumor regions. There are also possibilities that SGLTs are uniquely tied to some aspect of tumor biology in these regions, and play some role in disease progression. SGLTs could also contribute to some unique aspect of metabolism, as SGLTs expressed in certain regions of the cell could favor one metabolic pathway over another. These questions leave great potential for future work in the area of sodium glucose transporters in cancer.

The combination of dapa sensitive and SGLT2 protein staining in the xenografts marks the first time SGLT2 is implicated as a significant contributor to SGLT activity in cancer. Previously, antibodies for SGLT2 were not available, thus measurements of SGLT2 expression were few and limited to mRNA expression. The identification of SGLT2 expression in xenografts opens the door for more testing of SGLT2 expression in cancer; possibly assigning SGLT2 an even more prominent role than SGLT1 in tumor development. Clearly more work needs to be done in the area of SGLT expression, as SGLT1 has been the dominant protein tested up until this point.

Confident that SGLT2 is expressed and active in these cancer xenografts, we are now poised to conduct additional experiments to determine the dependence of cancer survival on SGLT2 activity, as well as experiments for establishing correlations between SGLT2 activity and disease characteristics and prognosis.

4 Activity of Glucose Transporters in Human Tumor Samples

4.1 Introduction

With SGLT activity established in animal xenografts, the next question to address was whether or not this SGLT activity is also present in tumors in human patients. Since the environment in the human body is significantly different than that in an immune compromised mouse, we couldn't immediately assume that success in animal models guarantees success in humans. Thus it was imperative for us to test Me-4FDG uptake in human tumors. As a preliminary test before conducting human scans, we obtained fresh tumor samples from surgery to test Me-4FDG uptake in live tissue samples. Similar to the *in vitro* cellular SGLT activity assays, incubating thin tumor sections with Me-4FDG with or without SGLT inhibition allowed us to confirm functional activity via autoradiography. Tumor sections were then tested for GLUT and SGLT protein expression, to see if the same heterogeneous tumor regions that were observed in the xenograft samples are also present in human tumors.

Having fresh tumor samples to section and test also gave us the ability to test the same tumor sample for both 2-FDG and Me-4FDG uptake by incubating adjacent tumor sections with either 2-FDG or Me-4FDG. The autoradiography images of each section were then compared to see if there are in fact different tumor regions that prefer either GLUTs or SGLTs for glucose consumption. As confirmation, SGLT and GLUT immunohistochemistry was used to see if protein expression matches the transporter activity measured by autoradiography, in the same manner as in the xenograft tests. Our goal was to determine if different tumor regions can be identified, which would open up the possibility for a wide variety of experiments testing for correlation of tumor metabolism with a variety of other factors, such as blood supply and regulator proteins.

4.2 Materials and Methods

4.2.1 Tumor samples

Tumor specimens freshly excised from patients were obtained from the UCLA Pathology department after pathological examination. Specimens were preserved in ice cold PBS while sliced to a thickness of roughly 300 microns using a Lancer Vibratome Series 1000 sectioning system and kept in numerical order. Slices with roughly similar shapes were used for uptake assays to simplify the comparison between tumor sections incubated in different conditions.

4.2.2 Me-4FDG/2-FDG uptake

Tumor sections were washed three times with ice cold PBS, then incubated in 200μL PBS with 10μCi of either 2-FDG or Me-4FDG, with or without inhibitors. For 2-FDG uptake, cytochalasin B was used as the inhibitor, while either dapa or phlorizin were used as inhibitor for Me-4FDG uptake. Tumor sections were incubated for 15 minutes; washed 3 times with ice cold PBS, then taken for autoradiography. Autoradiography film was exposed for anywhere from 1-15 minutes, depending on the strength of the signal, and analyzed as described previously with Fujifilm BAS-5000 image reader.

4.2.3 Immunohistochemistry

Immunohistochemistry was conducted as previously described in section 3. Tumor sections used in autoradiography were frozen in OTC, sliced into 10 micron sections with Leica CM3050S cryostat, then mounted onto glass slides and soaked in 10% formalin for fixation. Antigen retrieval was performed in citrate buffer at 85°C for 10 minutes for GLUT1 and GLUT3 staining.

4.3 GLUT vs SGLT activity in human tumor samples

Several tumor samples for both prostate cancer and pancreatic cancer were obtained for analysis. As shown in Figure 43, cytochalasin B completely inhibited 2-FDG uptake, indicating 2-FDG uptake in slices was specifically due to GLUT activity. While each of the specimen slices came out slightly differently, they were similar enough to compare one region to the adjacent one. Tested specimen samples showed both phlorizin or dapa sensitive Me-4FDG uptake as well as cytochalasin B sensitive 2-FDG uptake, similar to animal xenografts.
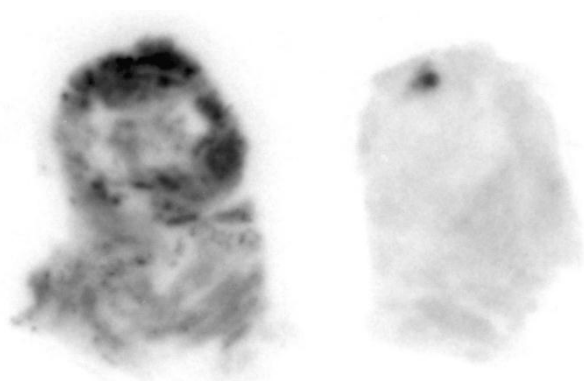
Figure 43: Sections from specimen PRCA3, taken from prostate cancer surgery, incubated with 2-FDG (left) and 2-FDG with cytochalasin B (right). Uptake of 2-FDG is completely inhibited by cytochalasin B in tissue samples.

One of the clearest samples tested was from pancreatic cancer sample PACA5, which showed both Me-4FDG and 2-FDG uptake. As shown in Figure 44, GLUT1 and GLUT3 staining correlate strongly with 2-FDG signal, with GLUT3 staining slightly stronger than GLUT1. SGLT2 staining conducted by Dr. Scafoglio also showed correlation with Me-4FDG uptake, which showed strong signal in the tumor sample.
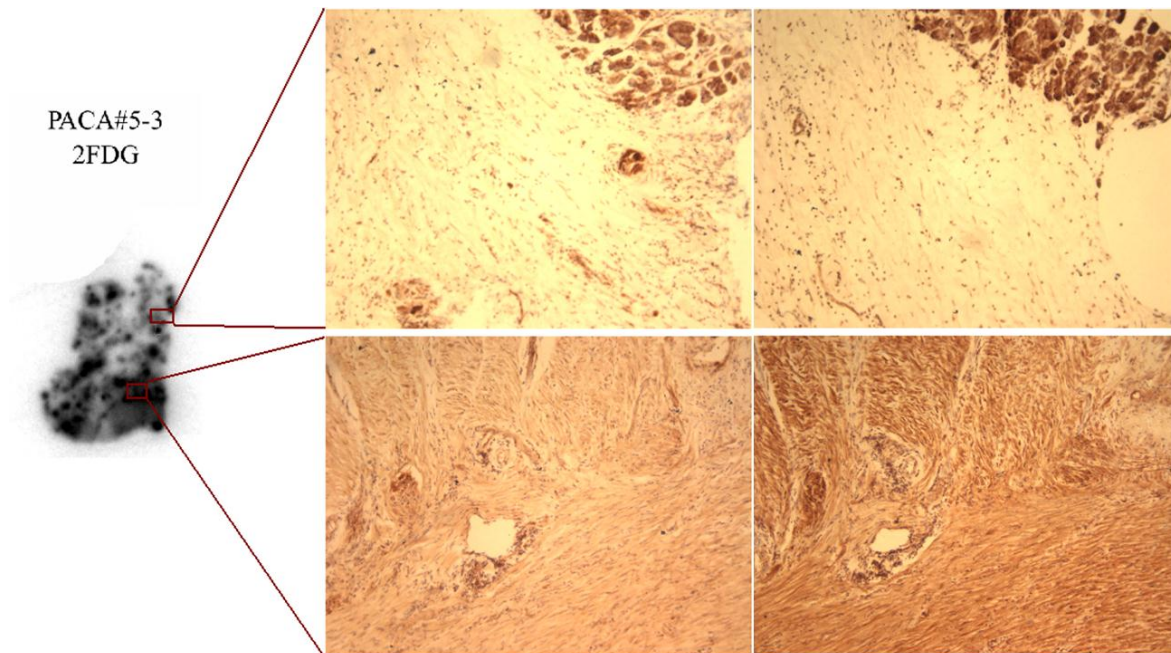
Figure 44: 2-FDG uptake and immunohistochemistry staining in 10 micron slices made from PACA5, section 3. GLUT3 staining (right) shows slightly stronger signal than GLUT1 staining (left), but in both cases staining correlates very strongly with 2-FDG uptake in autoradiography.

In the specimen samples examined from cancer surgeries, 2-FDG signal and Me-4FDG signal often overlapped, although not always. Samples were also inconsistent with regards to whether GLUT1 or GLUT3 correlated with 2-FDG signal, which is fairly reasonable given the diversity present within even the same cancer type. Despite these inconsistencies, these results mark the first instance of comparing SGLT activity with GLUT activity in tumor samples. The results also highlight the potential of using Me-4FDG in tumor imaging, as well as the contribution to tumor heterogeneity by both active and passive glucose transporters. We can now say with confidence that sodium glucose transporters are active in at least some human cancers to a level comparable to GLUTs, opening the door for further research examining the activity of SGLTs in cancer.

5 Future Work

With this work now demonstrating conclusively that sodium glucose transporters are expressed and active in cancer tumors, a wide variety of future experiments are possible. The most immediately promising experiment, currently underway, is testing SGLT inhibition as a potential treatment for cancer in mouse models with xenografts that show high Me-4FDG uptake. Several SGLT2 inhibitors are already in clinical trials for diabetes treatment and have shown to be safe in humans; the combination of a treatment that both lowers blood sugar levels and inhibits the active sodium glucose transporters capable of taking up glucose at low concentrations could prove to be extremely effective in limiting tumor growth. If SGLT2 activity does offer some level of survival benefit in cancer, SGLT2 inhibitors could soon emerge as a novel treatment for cancer.

Beyond animals, Me-4FDG now has the potential to be used more widely in human scans. There would be great potential in trials comparing Me-4FDG imaging in cancer to other conventional imaging such as MRI, CT, and PET scans using other molecular imaging probes. If it can be shown that Me-4FDG is diagnostically accurate for PET imaging, as is suggested by the animal scans we conducted, additional studies could be conducted comparing SGLT activity with patient prognosis and clinical outcomes. Until now, analyses relating SGLT to clinical outcomes have based solely on SGLT protein expression; functional imaging, however, can provide a faster and more reliable metric to use than traditional immunohistochemistry, leaving less uncertainty regarding the activity of the detected proteins. Particularly if it is shown that SGLT inhibition is an effective treatment for cancer, SGLT imaging could potentially allow oncologists to direct treatments that match PET scans for tumors with higher sodium glucose transporter activity.

There also remains much to be elucidated regarding these different tumor regions. While we have already seen that there are different tumor regions that utilize either SGLT or GLUT glucose consumption to greater extent, we have yet to link the preference of these transporters to any unique aspect of tumor biology. Previous work discussed earlier has already linked SGLT expression or activity to a variety of regulator proteins, such as EGFR, AMPK, and Bcl-2. Testing for the overexpression or activation of these various regulator proteins in tumors that have high or low Me-4FDG uptake could help establish these connections, and if so, it is possible Me-4FDG PET scans can provide some insight into regulator protein expression in tumors before tumors are surgically removed. The more information that can be gathered regarding a tumor before it is removed, the more directed subsequent tests on the tumor can be after it is excised.

The work currently being done on the expression of SGLTs in cancer is exciting and promising. With each new discovery, new opportunities open for the development of new potential imaging or treatment options. Sodium glucose transporters offer the unique benefit of being a transporting system that is easily identifiable by PET imaging and targetable for inhibition without significantly affecting the rest of the body. While it remains to be proven whether or not SGLTs play a vital, irreplaceable role in cancer survival, we now have reason to believe that at the very least they are functional and beneficial for at least some cancers.

Bibliography

1. De la Fuente, S. G. *et al.* Incidence of benign disease in patients that underwent resection for presumed pancreatic cancer diagnosed by endoscopic ultrasonography (EUS) and fine-needle aspiration (FNA). *J Gastrointest Surg* **14,** 1139–42 (2010)

2. Al-Sukhun, S. *et al.* Chemoradiotherapy in the treatment of regional pancreatic carcinoma: a phase II study. *Am J Clin Oncol* **26,** 543–9 (2003).

3. Yeo, T. P. *et al.* Assessment of "gene-environment" interaction in cases of familial and sporadic pancreatic cancer. *J Gastrointest Surg* **13,** 1487–94 (2009).

4. Vincent, A., Herman, J., Schulick, R., Hruban, R. H. & Goggins, M. Pancreatic cancer. *Lancet* **378,** 607–620 (2011).

5. Kawarada, Y. [JPS 5th ed. Classification of pancreatic cancer and JPS classification versus UICC classification]. *Nippon Rinsho* **64 Suppl 1,** 81–6 (2006).

6. Jung, K. W. *et al.* Clinicopathological aspects of 542 cases of pancreatic cancer: a special emphasis on small pancreatic cancer. *J Korean Med Sci* **22 Suppl,** S79–85   (2007).

7. Yamaguchi, K., Chijiiwa, K., Saiki, S., Nakatsuka, A. & Tanaka, M. "Mass-forming" pancreatitis masquerades as pancreatic carcinoma. *Int J Pancreatol* **20,** 27–35 (1996).

8. Krech, R. L. & Walsh, D. Symptoms of pancreatic cancer. *J Pain Symptom Manag.* **6,** 360–7 (1991).

9. Forsmark, C. E., Lambiase, L. & Vogel, S. B. Diagnosis of pancreatic cancer and prediction of unresectability using the tumor-associated antigen CA19-9. *Pancreas* **9,** 731–4   (1994).

10. Ni, X. G. *et al.* The clinical value of serum CEA, CA19-9, and CA242 in the diagnosis and prognosis of pancreatic cancer. *Eur J Surg Oncol* **31,** 164–9 (2005).

11. Goonetilleke, K. S. & Siriwardena, A. K. Systematic review of carbohydrate antigen (CA 19-9) as a biochemical marker in the diagnosis of pancreatic cancer. *Eur J Surg Oncol* **33,** 266–70 OD   (2007).

12. Chen, R., Pan, S., Brentnall, T. A. & Aebersold, R. Proteomic profiling of pancreatic cancer for biomarker discovery. *Mol Cell Proteomics* **4,** 523–33   (2005).

13. Goggins, M., Canto, M. & Hruban, R. Can we screen high-risk individuals to detect early pancreatic carcinoma? *J Surg Oncol* **74,** 243–8   (2000).

14. Brakenhielm, E. *et al.* Modulating metastasis by a lymphangiogenic switch in prostate cancer. *Int J Cancer* **121,** 2153–61 (2007).

15.   Schoder, H. & Larson, S. M. Positron emission tomography for prostate, bladder, and renal cancer. *Semin Nucl Med* **34,** 274–92 (2004).

16.   Hong, H., Zhang, Y., Sun, J. & Cai, W. Positron emission tomography imaging of prostate cancer. *Amino Acids* **39,** 11–27 (2009).

17.   Madu, C. O. & Lu, Y. Novel diagnostic biomarkers for prostate cancer. *J. Cancer* **1,** 150–177 (2010).

18.   Andriole, G. L. *et al.* Mortality results from a randomized prostate-cancer screening trial. *N. Engl. J. Med.* **360,** 1310–1319 (2009).

19.   Salami, S. S. *et al.* Combining urinary detection of TMPRSS2:ERG and PCA3 with serum PSA to predict diagnosis of prostate cancer. *Urol. Oncol. Semin. Orig. Investig.* **31,** 566–571 (2013).

20.   Gatenby, R. A. & Gillies, R. J. Why do cancers have high aerobic glycolysis? *Nat. Rev. Cancer* **4,** 891–899 (2004).

21.   Porporato, P. E., Dhup, S., Dadhich, R. K., Copetti, T. & Sonveaux, P. Anticancer targets in the glycolytic metabolism of tumors: a comprehensive review. *Front. Pharmacol.* **2,** 49 (2011).

22.   Granchi, C. & Minutolo, F. Anti-cancer agents counteracting tumor glycolysis. *ChemMedChem* **7,** 1318–1350 (2012).

23.   Williams, D. B. *et al.* Endoscopic ultrasound guided fine needle aspiration biopsy: a large single centre experience. *Gut* **44,** 720–6 (1999).

24.   Eloubeidi, M. A. *et al.* Endoscopic ultrasound-guided fine needle aspiration biopsy of patients with suspected pancreatic cancer: diagnostic accuracy and acute and 30-day complications. *Am J Gastroenterol* **98,** 2663–8 (2003).

25.   Anderson, M. A. *et al.* Endoscopic ultrasound is highly accurate and directs management in patients with neuroendocrine tumors of the pancreas. *Am J Gastroenterol* **95,** 2271–7 (2000).

26.   Agarwal, B., Abu-Hamda, E., Molke, K. L., Correa, A. M. & Ho, L. Endoscopic ultrasound-guided fine needle aspiration and multidetector spiral CT in the diagnosis of pancreatic cancer. *Am J Gastroenterol* **99,** 844–50   (2004).

27.   Mackie, C. R., Cooper, M. J., Lewis, M. H. & Moossa, A. R. Non-operative differentiation between pancreatic cancer and chronic pancreatitis. *Ann Surg* **189,** 480–7   (1979).

28. Chung, S. M. Safety issues in magnetic resonance imaging. *J Neuroophthalmol* **22,** 35–9 (2002).

29. Bearcroft, P. W. & Lomas, D. J. Magnetic resonance cholangiopancreatography. *Gut* **41,** 135–7 (1997).

30. Adamek, H. E. *et al.* Pancreatic cancer detection with magnetic resonance cholangiopancreatography and endoscopic retrograde cholangiopancreatography: a prospective controlled study. *Lancet* **356,** 190–3 (2000).

31. Langen, K. J. *et al.* SPECT studies of brain tumors with L-3-[123I] iodo-alpha-methyl tyrosine: comparison with PET, 124IMT and first clinical results. *J. Nucl. Med.* **31,** 281–286 (1990).

32. Mariani, G. *et al.* A review on the clinical uses of SPECT/CT. *Eur. J. Nucl. Med. Mol. Imaging* **37,** 1959–1985 (2010).

33. Heinrich, S. *et al.* Positron emission tomography/computed tomography influences on the management of resectable pancreatic cancer and its cost-effectiveness. *Ann Surg* **242,** 235–43 (2005).

34. Kauhanen, S. P. *et al.* A prospective diagnostic accuracy study of 18F-fluorodeoxyglucose positron emission tomography/computed tomography, multidetector row computed tomography, and magnetic resonance imaging in primary diagnosis and staging of pancreatic cancer. *Ann Surg* **250,** 957–63 (2009).

35. Quon, A. *et al.* Initial evaluation of 18F-fluorothymidine (FLT) PET/CT scanning for primary pancreatic cancer. *Eur J Nucl Med Mol Imaging* **35,** 527–31 (2008).

36. Schmid, D. T. *et al.* Fluorocholine PET/CT in patients with prostate cancer: initial experience. *Radiology* **235,** 623–8 (2005).

37. De Jong, I. J., Pruim, J., Elsinga, P. H., Vaalburg, W. & Mensink, H. J. Preoperative staging of pelvic lymph nodes in prostate cancer by 11C-choline PET. *J Nucl Med* **44,** 331–5 (2003).

38. Shreve, P. D., Grossman, H. B., Gross, M. D. & Wahl, R. L. Metastatic prostate cancer: initial findings of PET with 2-deoxy-2-[F-18]fluoro-D-glucose. *Radiology* **199,** 751–6 (1996).

39. Oyama, N. *et al.* 11C-acetate PET imaging of prostate cancer. *J Nucl Med* **43,** 181–6 (2002).

40. Zeisel, S. H. Dietary choline: biochemistry, physiology, and pharmacology. *Annu Rev Nutr* **1,** 95–121 (1981).

41. Bhakoo, K. K., Williams, S. R., Florian, C. L., Land, H. & Noble, M. D. Immortalization and transformation are associated with specific alterations in choline metabolism. *Cancer Res* **56,** 4630–5 (1996).

42. Krause, B. J., Souvatzoglou, M. & Treiber, U. Imaging of prostate cancer with PET/CT and radioactively labeled choline derivates. *Urol Oncol* **4**, 427-35 (2013)

43. Larson, S. M. *et al.* Tumor localization of 16beta-18F-fluoro-5alpha-dihydrotestosterone versus 18F-FDG in patients with progressive, metastatic prostate cancer. *J Nucl Med* **45,** 366–73 (2004).

44. Reivich, M. *et al.* Glucose metabolic rate kinetic model parameter determination in humans: the lumped constants and rate constants for [18F]fluorodeoxyglucose and [11C]deoxyglucose. *J Cereb Blood Flow Metab* **5,** 179–92 (1985).

45. Wright, E. M., Loo, D. D. F. & Hirayama, B. A. Biology of human sodium glucose transporters. *Physiol Rev* **91,** 733–94 OD – 2011/04/30 (2011).

46. Chao, E. C. & Henry, R. R. SGLT2 inhibition — a novel strategy for diabetes treatment. *Nat. Rev. Drug Discov.* **9,** 551–559 (2010).

47. Hardman, T. C. & Dubrey, S. W. Development and potential role of type-2 sodium-glucose transporter inhibitors for management of type 2 diabetes. *Diabetes Ther* **2,** 133–45 (2011)

48. Yu, A. S. *et al.* Regional distribution of SGLT activity in rat brain in vivo. *Am. J. Physiol. Cell Physiol.* **304,** C240–7 (2013).

49. Yu, A. S. *et al.* Functional expression of SGLTs in rat brain. *Am. J. Physiol. Cell Physiol.* **299,** C1277–C1284 (2010).

50. Diez-Sampedro, A. *et al.* A glucose sensor hiding in a family of transporters. *Proc Natl Acad Sci U S A* **100,** 11753–8 (2003).

51. Grempler, R. *et al.* Functional characterisation of human SGLT-5 as a novel kidney-specific sodium-dependent sugar transporter. *FEBS Lett* **586,** 248–53 (2012)

52. Grempler, R. *et al.* Empagliflozin, a novel selective sodium glucose cotransporter-2 (SGLT-2) inhibitor: characterisation and comparison with other SGLT-2 inhibitors. *Diabetes Obes Metab* **14,** 83–90 (2011)

53. Nelson, J. A. & Falk, R. E. The efficacy of phloridzin and phloretin on tumor cell growth. *Anticancer Res* 2287–2292 (1993).

54. Blessing, A. *et al.* Sodium / Glucose Co-transporter 1 Expression Increases in Human Diseased Prostate. *J Cancer Sci Ther* **4,** 306–312 (2012).

55. Weihua, Z. *et al.* Survival of cancer cells is maintained by EGFR independent of its kinase activity. *Cancer Cell* **13,** 385–93 (2008).

56. Ren, J. *et al.* EGFR-SGLT1 interaction does not respond to EGFR modulators, but inhibition of SGLT1 sensitizes prostate cancer cells to EGFR tyrosine kinase inhibitors. *Prostate* 1–9 (2013).

57. Nicholson, R. I., Gee, J. M. & Harper, M. E. EGFR and cancer prognosis. *Eur J Cancer* **37 Suppl 4,** S9–15 (2001).

58. Casneuf, V. F. *et al.* Expression of SGLT1, Bcl-2 and p53 in primary pancreatic cancer related to survival. *Cancer Invest* **26,** 852–9 (2008).

59. Boucher, M. J. *et al.* MEK/ERK signaling pathway regulates the expression of Bcl-2, Bcl-X(L), and Mcl-1 and promotes survival of human pancreatic cancer cells. *J Cell Biochem* **79,** 355–69 (2000).

60. Yin, X. M., Oltvai, Z. N., Veis-Novack, D. J., Linette, G. P. & Korsmeyer, S. J. Bcl-2 gene family and the regulation of programmed cell death. *Cold Spring Harb Symp Quant Biol* **59,** 387–93 (1994).

61. Waters, J. S. *et al.* Phase I clinical and pharmacokinetic study of bcl-2 antisense oligonucleotide therapy in patients with non-Hodgkin's lymphoma. *J Clin Oncol* **18,** 1812–23 (2000).

62. Kang, M. H. & Reynolds, C. P. Bcl-2 inhibitors: targeting mitochondrial apoptotic pathways in cancer therapy. *Clin Cancer Res* **15,** 1126–32 (2009).

63. Tse, C. *et al.* ABT-263: a potent and orally bioavailable Bcl-2 family inhibitor. *Cancer Res* **68,** 3421–8 (2008).

64. O'Brien, S. M. *et al.* Phase I study of obatoclax mesylate (GX15-070), a small molecule pan-Bcl-2 family antagonist, in patients with advanced chronic lymphocytic leukemia. *Blood* **113,** 299–305 (2009).

65. Lai, B. *et al.* Overexpression of SGLT1 is correlated with tumor development and poor prognosis of ovarian carcinoma. *Arch. Gynecol. Obstet.* **285,** 1455–1461 (2012).

66. Delezay, O. *et al.* Characterization of an electrogenic sodium/glucose cotransporter in a human colon epithelial cell line. *J. Cell. Physiol.* **163,** 120–128 (1995).

67. Bissonnette, P. *et al.* Kinetic separation and characterization of three sugar transport modes in Caco-2 cells. *Am. J. Physiol.* **270,** G833–G843 (1996).

68.   Guo, G. F. *et al.* Overexpression of SGLT1 and EGFR in colorectal cancer showing a correlation with the prognosis. *Med Oncol* **28 Suppl 1,** S197–203 (2010)

69.   Huber, S. M., Misovic, M., Mayer, C., Rodemann, H. P. & Dittmann, K. EGFR-mediated stimulation of sodium/glucose cotransport promotes survival of irradiated human A549 lung adenocarcinoma cells. *Radiother Oncol* **103,** 373–9 (2012)

70.   Ishikawa, N., Oguri, T., Isobe, T., Fujitaka, K. & Kohno, N. SGLT gene expression in primary lung cancers and their metastatic lesions. *Jpn. J. Cancer Res.* **92,** 874–879 (2001).

71.   Helmke, B. M., Reisser, C., Idzko, M., Dyckhoff, G. & Herold-Mende, C. Expression of SGLT-1 in preoplastic and neoplastic lesions of the head and neck. *Oral Oncol.* **40,** 28–35 (2004).

72.   Hanabata, Y., Nakajima, Y., Morita, K., Kayamori, K. & Omura, K. Coexpression of SGLT1 and EGFR is associated with tumor differentiation in oral squamous cell carcinoma. *Odontology* **100,** 156–163 (2012).

73.   Perez, M. *et al.* MAP17 and SGLT1 Protein Expression Levels as Prognostic Markers for Cervical Tumor Patient Survival. *PLoS One* **8,** (2013).

74.   Sridhar, S. S., Seymour, L. & Shepherd, F. A. Inhibitors of epidermal-growth-factor receptors: a review of clinical research with a focus on non-small-cell lung cancer. *Lancet Oncol* **4,** 397–406 (2003).

75.   Logsdon, C. D. *et al.* Molecular profiling of pancreatic adenocarcinoma and chronic pancreatitis identifies multiple genes differentially regulated in pancreatic cancer. *Cancer Res* **63,** 2649–57 (2003).

76.   Bashyam, M. D. *et al.* Array-based comparative genomic hybridization identifies localized DNA amplifications and homozygous deletions in pancreatic cancer. *Neoplasia* **7,** 556–62 (2005).

77.   Atala, A. Re: PC3 is a cell line characteristic of prostatic small cell carcinoma. *J Urol* **188,** 325 (2012)

78.   Pascal, L. E. *et al.* Lineage relationship of prostate cancer cell types based on gene expression. *BMC Med Genomics* **4,** 46 (2011)

79.   Thalmann, G. N. *et al.* Androgen-independent cancer progression and bone metastasis in the LNCaP model of human prostate cancer. *Cancer Res* **54,** 2577–81 (1994).

80.   Effert, P., Beniers, A. J., Tamimi, Y., Handt, S. & Jakse, G. Expression of glucose transporter 1 (Glut-1) in cell lines and clinical specimens from human prostate adenocarcinoma. *Anticancer Res* **24,** 3057–63 (2004).

81. Wright, E. M., Hirsch, J. R., Loo, D. D. & Zampighi, G. A. Regulation of Na+/glucose cotransporters. *J Exp Biol* **200,** 287–93 (1997).

82. Ghezzi, C. & Wright, E. M. Regulation of the human Na+-dependent glucose cotransporter hSGLT2. *Am J Physiol Cell Physiol* **303,** C348–54 (2012)

83. Murata, Y. *et al.* Correlations between 18F-FDG uptake by bone marrow and hematological parameters: measurements by PET/CT. *Nucl Med Biol* **33,** 999–1004 (2006).